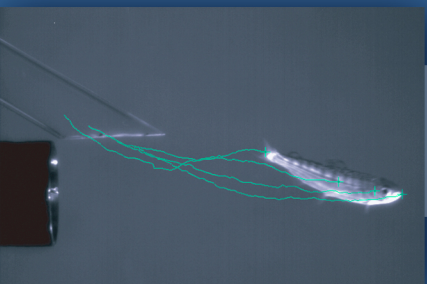**Pacific Northwest National Laboratory**
Operated by Battelle for the
U.S. Department of Energy

Study of Fish Response Using Particle Image Velocimetry and High-Speed, High-Resolution Imaging

Z. Deng
M.C. Richmond
G.R. Guensch
R.P. Mueller
Pacific Northwest National Laboratory

October 2004

U.S. Department of Energy
Energy Efficiency and Renewable Energy

Wind and Hydropower Technologies

Bringing you a prosperous future where energy is clean, abundant, reliable, and affordable

Study of Fish Response Using Particle Image Velocimetry and High-Speed, High-Resolution Imaging

Zhiqun Deng
Marshall C. Richmond
Gregory R. Guensch
Robert P. Mueller

October 2004

Pacific Northwest National Laboratory
Richland, Washington 99352

Executive Summary

Fish swimming has fascinated both engineers and fish biologists for decades. Digital particle image velocimetry (DPIV) and high-speed, high-resolution digital imaging are recently developed analysis tools that can help engineers and biologists better understand how fish respond to turbulent environments. We undertook the studies described here to evaluate DPIV for the US Department of Energy (DOE) Hydropower Program. The studies included a review of existing literature on DPIV, preliminary studies to test the feasibility of using DPIV conducted at our Flow Biology Laboratory in Richland, Washington September through December 2003, and applications of high-speed, high-resolution digital imaging with advanced motion analysis to investigations of fish injury mechanisms in turbulent shear flows and bead trajectories in laboratory physical models. The results of these studies are reported here. We drew several conclusions based on these studies, which are summarized as recommendations for proposed research at the end of this report.

We reviewed the existing literature on PIV studies of fish swimming and found that most of these studies focused on the performance evaluation of freely swimming fish. Technological advances over the last decade, especially the development of digital particle image velocimetry (DPIV) technique, make possible whole-field, more accurate, quantitative descriptions of the instantaneous flow patterns adjacent to the fish and in the wake behind the fins and tail, which are imperative to decode the mechanisms of drag reduction and propulsion efficiency, and improve the understanding of fish injury mechanisms in extreme hydraulic environments such as high shear/turbulence, and collision.

For flows generated by different organisms, the related scales and flow regimes vary significantly. For small Reynolds numbers, viscosity dominates; for very high Reynolds numbers, inertia dominates, and three-dimensional complexity occurs. The majority of previous investigations dealt with the lower end of the Reynolds number range. The fish of our interest, such as rainbow trout and spring and fall Chinook salmon, fall into the middle range, in which neither viscosity nor inertia is negligible, and three-dimensionality has yet to dominate.

Our feasibility tests demonstrate the applicability of PIV to flows around fish. These tests have shown unsteady vortex shedding in the wake, high-vorticity region, and high-stress region, with the highest in the pectoral area. This evidence supports the observations by Neitzel et al. (2000); Deng et al. (2004a) that the operculum are the most vulnerable to damage from the turbulent shear flow, because they are easily pried open, and high vorticity and shear stress can lift and tear off scales, rupture or dislodge eyes, and damage gills. In addition, the unsteady behavior of the vortex shedding in the wake implies that injury to fish by the instantaneous flow structures would likely be much higher than the injury level estimated using the average values of the dynamics parameters.

We also employed high-speed high-resolution digital cameras and advanced motion analysis technique to better quantify the kinematic and dynamic parameters associated with the exposure of fish or Sensor Fish to turbulent shear flow, and the accuracy of bead tracking (emulating fish in prototype) in physical models. The computed parameters included the velocity, acceleration,

jerk, bending angle of the body, and bulk force on the object. The injury type and severity were then related to fish size (length and mass), exposure strain rate, and the magnitude of the computed kinematic and dynamic parameters. The test results demonstrate the applicability of high-speed, high-resolution imaging with advanced motion analysis to the study of biological response of fish in hydraulic environments.

Based on existing literature, our technological capability, and relevance and practicability to the US Department of Energy's Hydropower Program, we identified three major research areas of interest:

1. Collisions

2. High shear/turbulence

3. Sensor Fish

We propose that the highest priority is to characterize the kinematic response of fish and sensor fish to different turbulent environments such as high shear/turbulence and hydrodynamic disturbances created by solid structures such as deflector and turbine runner blade. The next priority is to correlate the responses of live fish and sensor fish.

Grid turbulence and Kármán vortex street will be employed to map the boundary layers over fish and investigate the effects of environmental disturbances on the swimming performance of fish, because they are well established and documented in engineering literature and are representative of fish's swimming environments. Extreme conditions characteristic of turbine environments, such as strong shear environment and collision, will be investigated in detail.

Through controlled laboratory studies using DPIV and high-speed, high-resolution digital imaging with advanced motion analysis, fish injury mechanisms, including high shear/turbulence and mechanical injuries will be evaluated in isolation. The major goals are to gain first-hand knowledge of the biological effects under such extreme hydraulic environments in which fish could lack the capability to overcome the perturbations and be vulnerable to injury and better understand field results by integrating the laboratory studies with the responses of the Sensor Fish Device. More importantly, this research would provide well-defined validation cases and boundary conditions for biological response modeling in order to simulate the complex hydraulic environments in advanced hydropower systems and their effects on fish, greatly enhancing the potential to use computational fluid dynamics as a bio-hydraulic design alternative.

Acknowledgments

Contents

Figures

1.0 Introduction

A better understanding of the biological responses of juvenile fish in turbulent hydraulic environments could lead to more fish-friendly advanced turbine designs. Digital particle image velocimetry (DPIV) is a recently developed technology that could aid in that understanding. Motion-tracking from video data is becoming a common experimental tool, but high-speed video studies of fish injuries are less common. In late 2003 and 2004 Pacific Northwest National Laboratory undertook an evaluation of PIV and applicability of high-speed, high-resolution imaging with advanced motion analysis to the study of biological response of fish in hydraulic environments for the US Department of Energy Hydropower Program. This evaluation, described in this report, included four components: a literature review of existing PIV studies, laboratory studies conducted by PNNL at its fisheries laboratories in late 2003 to test the feasibility of PIV for mapping velocity, vorticity and stress regions around a fish in turbulent shear flows, applicability of high-speed, high-resolution imaging with advanced motion analysis, and a compilation of recommendations for future research based on PNNL's findings.

1.1 Background

Fish swimming has been of great interest to both propulsion engineers and fish biologists for several decades. For engineers, fish locomotory mechanism, employing a rhythmic unsteady motion of the body and fins, offers a different perspective from existing aquatic engineering vehicles. Progress in the study of fish locomotion could enhance our understanding of the fundamental principles of aquatic propulsion and stability, and leading to improvements of the design and performance of aquatic vehicles. For fish biologists, it is imperative to have advanced knowledge on how fish react to environmental turbulence and other hydrodynamic disturbances to improve swimming performance and avoid injury, in order to make environmentally sound management decisions about turbine design, stream design, habitat management, and fish passageways.

The biological responses of juvenile fish in the turbine environment are particularly important for the design of fish-friendly advanced turbine systems. Injuries and mortality of fish that pass through hydroelectric turbines can result from several mechanisms, such as rapid and extreme pressure changes, shear stress, turbulence, strike, cavitation and grinding (Čada et al., 1997). Several laboratory studies have been conducted to establish the biological criteria for fish injury and mortality by quantifying the hydraulic forces (Neitzel et al. 2000; Guensch et al. 2002; Deng et al. 2004a). In these studies, acceleration, jerk, and force were correlated with injury. However, due to the difficulty in detailing the complex fluid/solid interaction, quantification of fish injury mechanisms in turbine environments has often depended more on numerical modelling than on direct measurements (Čada, 2001).

Jones and Sotiropoulos (2002) employed unsteady large-eddy simulations (LES) to compute the turbulent shear flows in the laboratory studies and carried out particle tracking studies to analyze the computed flow fields from the Lagrangian point of view, that is, how a fish is transported

by and interacting with the turbulent flow. They concluded that the actual flow environment experienced by the fish is vastly more complicated than that described by the mean flow.

In addition, dominant, large-scale, unsteady vortices exist in the flows of some regions of hydropower plants such as draft tubes and tailraces. Carlson (2001) found that these vortices could have important biological effects as they could disorient passing fish and result in increased injury or indirect mortality rates due to predation. Furthermore, these complex flow structures could create zones of high instantaneous shear stress and turbulence, thus contributing to additional fish injuries.

Technological advances over the last decade, especially in digital particle image velocimetry (DPIV), make possible accurate, quantitative descriptions of flow patterns in the vicinity of the fish and the wakes behind the fins and tail, which are essential to decode the mechanisms of drag reduction and propulsive efficiency. PIV technique provides an ideal approach for investigation of fish behavior in turbulent flows because it offers a whole-field view of the instantaneous flow field in a quantitative fashion. This allows the user to examine the presence of vortex structures and their influence, and obtain instantaneous vorticity, turbulence, and shear stress fields quantitatively and globally. These unique capabilities, plus high-speed, high-resolution imaging with advanced motion analysis, provide a powerful diagnostic tool for examining the nature of complex flows that offers the ability to validate the numerical codes and improve the accuracy of the predictive models.

1.2   Objectives

The objectives of the studies reported here are to

1. Conduct a review of existing literature on DPIV.

2. Conduct preliminary studies to test the feasibility of using DPIV conducted at PNNL's fisheries laboratories in Richland, Washington.

3. Use high-speed high-resolution imaging and advanced motion analysis technique to further improve the quantifications of hydrodynamic parameters.

4. Summarize results and develop a list of recommendations for future research.

With PIV overcoming many disadvantages of traditional experimental methods and proven very useful to study flow around fish, our motivations for Hydropower program are to: 1) Measure forces on fish caused by shear and turbulence; 2) Learn about the mechanisms of underwater collision; 3) Learn about how fish swim or fail to swim in turbulence of a range of intensity and scale; 4) Integrate the laboratory results with CFD modeling and Sensor Fish tests to better understand field data.

1.3   Overview of the Report

Chapter 2 provides an overview of the PIV and describes previous PIV studies. Chapter 3 describes the PIV feasibility study conducted by PNNL in late 2003. Chapter 4 discusses the application of High-Speed, High-Resolution Digital Imaging and Advanced Motion Analysis to studies of fish response. Chapter 5 lists recommendations for future studies based on our findings in the literature review and laboratory feasibility study. Chapter 6 provides conclusions. Chapter 7 is references. A compact disc containing video examples of results from our laboratory studies is also provided. The five video clips show instantaneous velocity vector field, instantaneous vorticity contour map , and instantaneous shear exposure strain contour map, and advanced motion analysis of fish and Sensor Fish. The velocity vectors are overlapped in the vorticity and exposure strain contour maps to better visualize the vortical structures.

2.0 Literature Review of PIV Studies on Fish

2.1 Fundamentals of Particle Image Velocimetry

During the last century, many point-wise velocity measurement techniques have been well developed, such as pitot tubes, hot-wire anemonmetry (HWA), laser doppler anemonetry (LDA), and acoustic doppler velocimetry (ADV). These techniques permit velocity measurement at a single spatial point only, thus they are unable to capture to instantaneous spatial structure of the flow. To obtain information about the spatial structure of a flow field, Taylor frozen hypothesis (Batchelor 1967) is normally assumed, i.e., advection contributed by turbulent circulations themselves is small and that therefore the advection of a field of turbulence past a fixed point can be taken to be entirely due to the mean flow.

In contrast to those traditional single-point velocity measurement techniques, Particle Image Velocimetry (PIV) is a state-of-the-art, whole-flow-field optical technique, providing instantaneous velocity vector measurements in a whole plane, and use of a stereoscopic approach permits instantaneous measurement of all three velocity components, resulting in real-time 3-D flow structures in areas of interest.

A typical configuration of a digital PIV system is shown in Figure 2.1. To measure the velocity of the fluid, the flow is seeded with small tracer particles that follow the fluid faithfully. A "plane" of the flow is illuminated by a thin sheet of light, usually laser light, and the images of the tracer particles within the "plane" are recorded twice with very small time delay Δt onto either a film (photographic or holographic) or a CCD (charge-coupled device) array. The fluid motion is represented by the displacement of the particles $\Delta \mathbf{X}$, and the first-order velocity estimate is

$$\mathbf{u} = \frac{\Delta \mathbf{X}}{\Delta t}, \tag{2.1}$$

where Δt is the time delay between the two recordings and $\Delta \mathbf{X}$ is the corresponding average displacement of the tracer particles in the fluid (Adrian 1991). A typical PIV image is shown in Figure 2.2.

Particle images are analyzed by subdividing the image into small interrogation spots as illustrated in Figure 2.3. To obtain accurate velocity measurements, each interrogation region should contain many particle-image pairs (Keane and Adrian 1992). Because the displacement is greater than the mean spacing between particle images, it is almost impossible to find individual matching pairs. Therefore, a statistical method, usually correlation analysis, is used to acquire the particle displacement. By computing the spatial auto-correlation for double-exposure single-frame images or cross-correlation for double-exposure double-frame images, the location of the displacement-correlation peak yields the average particle displacement. In the case of auto-correlation analysis, the two peaks centered around the self-correlation peak are the "true" displacement-correlation peaks and a 180-degree directional ambiguity occurs due to the symmetry of the auto-correlation. In comparison, in the case of cross-correlation, there is only one peak, the "true" displacement-
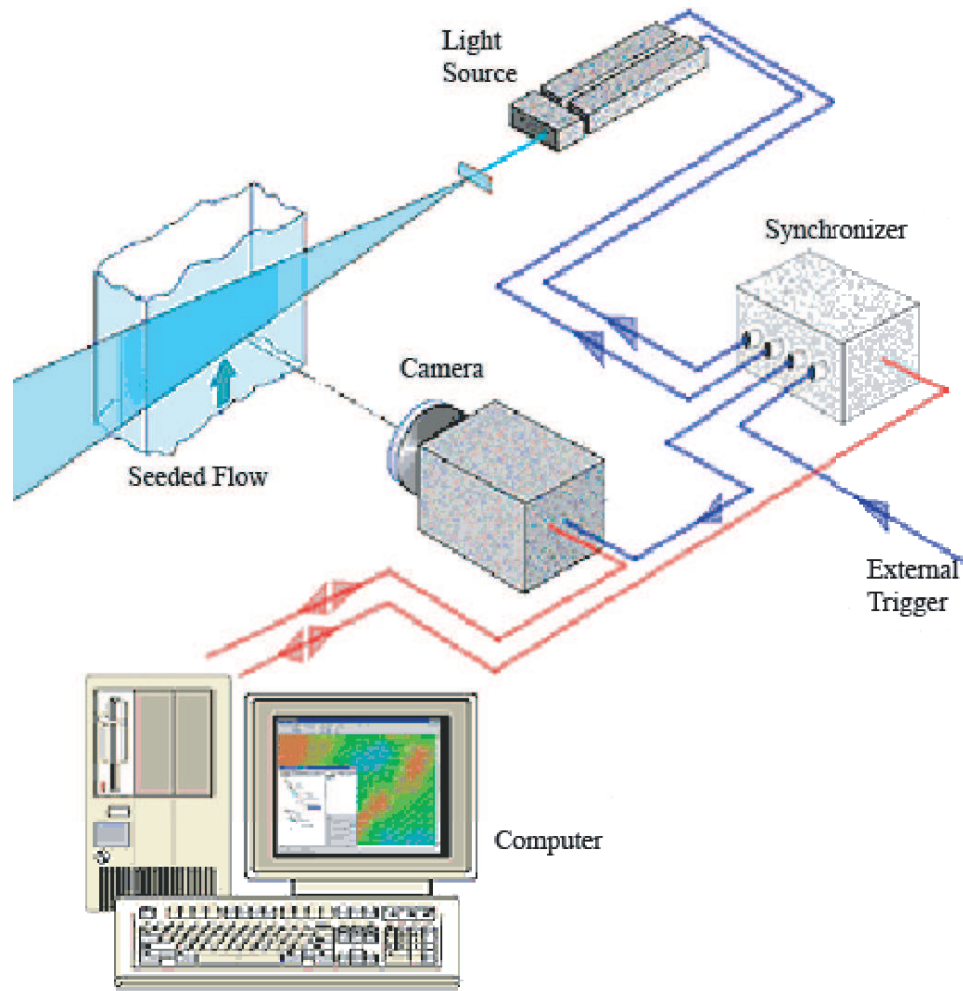
Figure 2.1. A typical configuration of a digital PIV system

correlation peak, and no directional ambiguity needs to be resolved. Repeating this procedure for all the interrogation spots and dividing the displacement with the time delay between the two recordings produce a raw velocity vector field. Applying validation algorithms to the raw vector maps, the erroneous vectors are detected and removed. Further analysis of these validated vectors will produce streamlines, vorticity, stress, turbulence intensity etc.

Since its establishment, PIV has been applied to many areas of research, including micro-scale flows and extreme conditions. Figure 2.4 demonstrates the PIV measurements in a 30 μm $\times$ 300 μm micro-channel (Meinhart et al. 1999). The resulting velocity fields have a spatial resolution of 13.6 μm $\times$ 0.9 μm in the streamwise and wall-normal directions, respectively. For applications in extreme conditions, Figures 2.5 and 2.6 show instantaneous flow patterns in a simulated solid rocket motor combustion chamber (Deng et al. 2002) and flow entrainment created by the emerging hot jet in the exhaust (Adrian et al. 2003).

More details about fundamentals of PIV can be found in Adrian (1991) and Raffel et al. (1998), and a complete bibliography was complied by Adrian (1996).

6
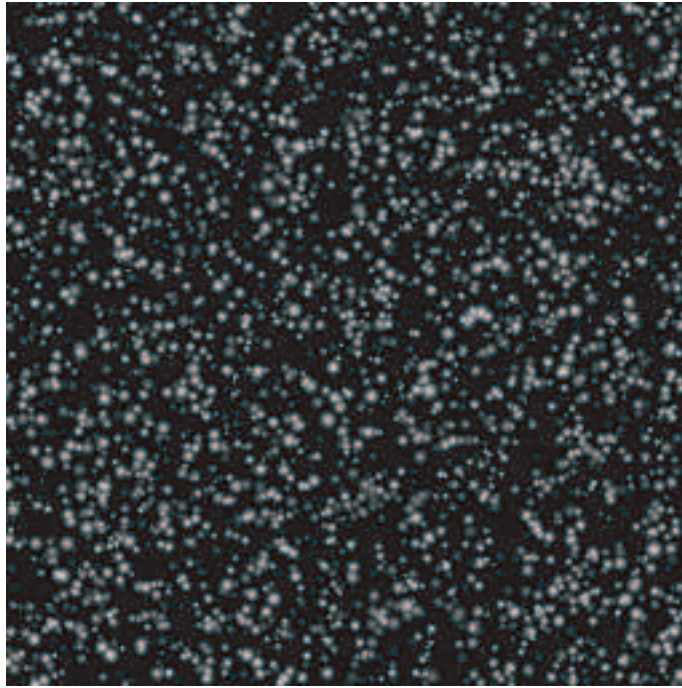
Figure 2.2. A typical PIV image obtained with a CCD camera.
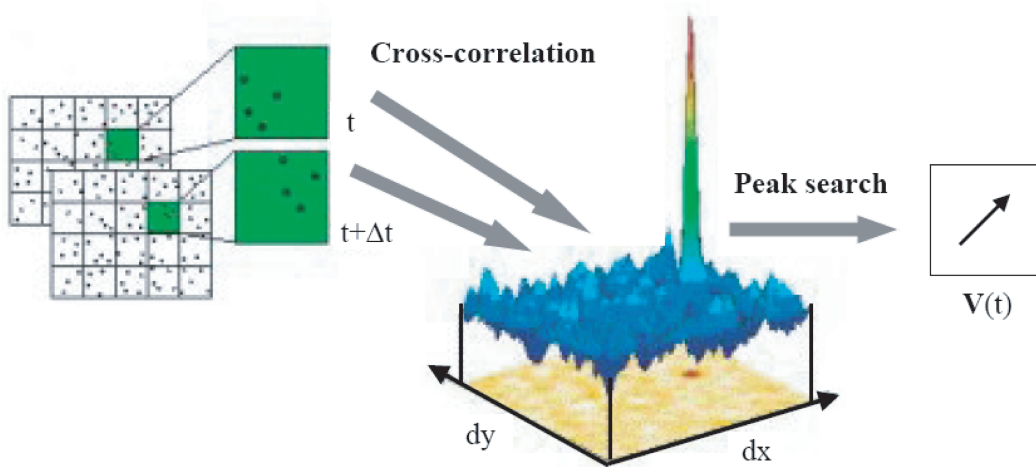
Figure 2.3. Cross-correlation for PIV images.
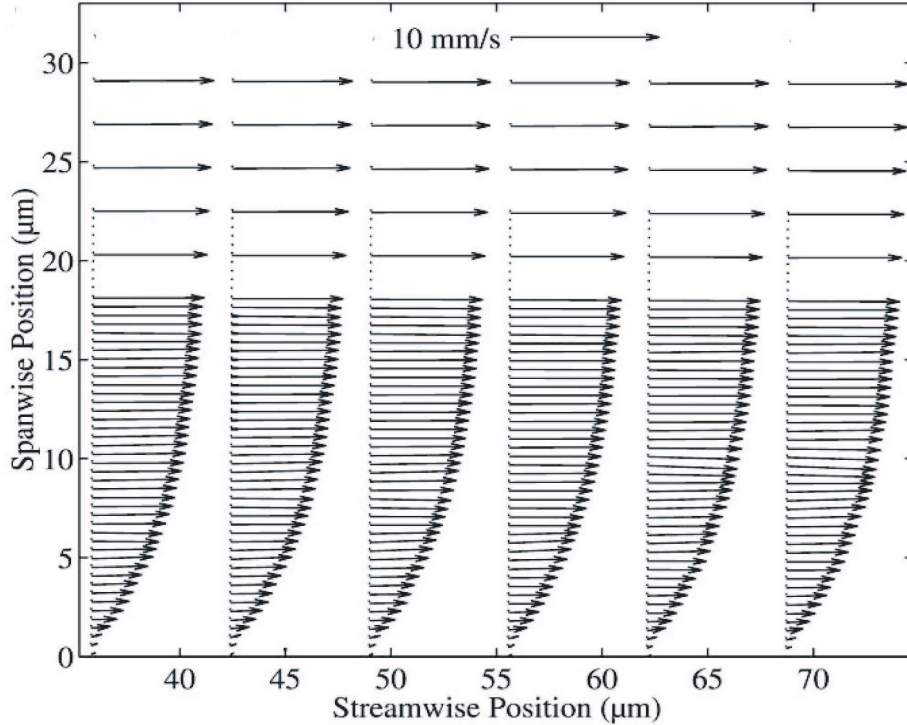
Figure 2.4. Ensemble-averaged velocity vector field measured in a $30 \, \mu\text{m} \times 300 \, \mu\text{m}$ micro-channel with a spatial resolution of $13.6 \, \mu\text{m} \times 0.9 \, \mu\text{m}$ in the streamwise and wall-normal directions, respectively (Meinhart et al. 1999).

2.2 Previous studies of fish swimming using PIV

Many experimental investigations of animal-generated flows have been conducted using PIV since this technique was applied to behavioral biomechanics. PIV, especially digital particle image velocimetry (DPIV), has proved to be a powerful tool and able to provide profound insight for the study of animal-generated flows such as swimming, pumping and feeding currents, etc., even though extra caution is needed to make sure that the normal behavior of the animals is not interrupted by the optical setup (Stamhuis and Videler 1995; Stamhuis et al. 2002).

For flows generated by different organisms, the related scales and flow regimes vary significantly. As shown in Figure 2.7, the Reynolds numbers ($Re = UL/\mu$) associated with the interaction between aquatic organisms and water range from 10^{-6} to 10^{9}. Accordingly, the associated flow regimes change from a predominantly viscous regime to an inertial regime (Videler 1993). Table 2.1 lists some previous studies covering this wide Re range.

Van Duren and Videler (2003) and Van Duren et al. (2003) measured the flow field around feeding and escaping adult copepod at $0.1 < Re < 100$ and computed vorticity and rate of energy dissipation. They found that the average rate of energy dissipation within the copepod's volume of influence was several times higher than the levels of turbulent energy dissipation the copepod generally encounters in its natural environment, and turbulence has no substantial effect on the fish even in highly turbulent environment.

8

Table 2.1. Previous particle image velocimetry studies of animal-generated flows.

Author(s)	Year	Species	Re	Swimming velocity (m/s)	Body length, L (mm)
Müller et al.	1997	Mullet	$\approx 30,000$	0.175	120
Stamhuis and Videler	1998	Shrimp	≈ 200	0.002	40
Drucker and Lauder	1999	Bluegill sunfish		0.1–0.3	203
Drucker and Lauder	2000	Black surfperch		0.21–0.62	208
Hanke et al.	2000	Goldfish		0.05–0.21	60 and 100
Liao and Lauder	2000	White sturgeon		0.3–0.37	250-310
Muller et al.	2000	Zebra danios	100–5,000	0.176	4 and 35
Drucker and Lauder	2001a	Bluegill sunfish		0.11	220
Drucker and Lauder	2001b	Bluegill sunfish		0.11 and 0.23	210
Muller et al.	2001	Eel	$\approx 30,000$	0.1–0.15	100
Anderson et al.	2001	Scup, dogfish	$3 \times 10^3 - 3 \times^5$	0.03-0.65	195 and 444
Stamhuis et al.	2002	Animals	$10^{-2}1-10^5$	0.002–0.2	
Nauen and Lauder	2002a	Chub mackerel		0.24–0.57	200-260
Nauen and Lauder	2002b	Rainbow trout		0.20–0.26	165–215
Van Duren and Videler	2003	Copepod	0.1–100	0.002–0.012	1.2
Liao et al.	2003b	Rainbow trout	5,000–40,000	0.25 and 0.45	100
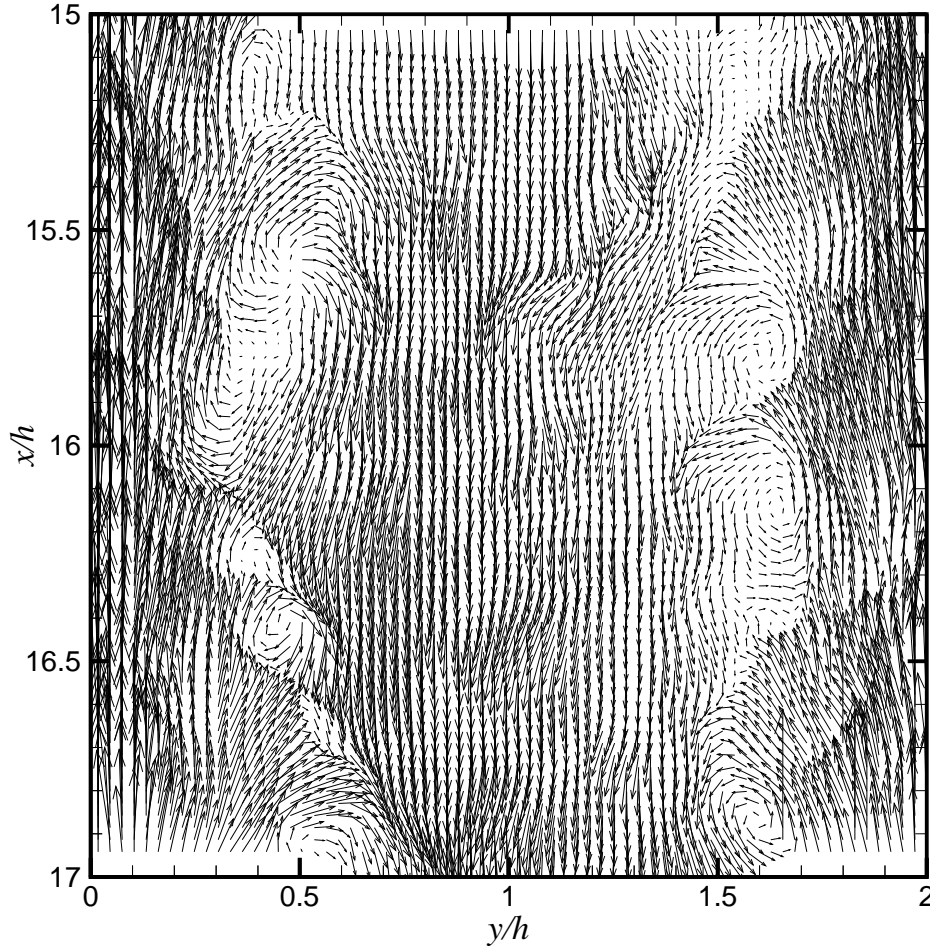
Figure 2.5. An example of instantaneous velocity vector maps in a simulated solid rocket motor combustion chamber with propellants injected from both sides and the core flow direction being downward (Deng et al. 2002).

Stamhuis and Videler (1998) measured the ventilation flow adjacent to a tube-dwelling shrimp at a Reynolds number of approximately 200 and evaluated the energetic consequences of pulsating and steady flows for several tube configurations.

Muller et al. (2000) studied the hydrodynamics of unsteady swimming and effects of body length on zebra danio larvae and adult fish, which swim in a burst-and-coast style. The body lengths of the larvae and adult fish were approximately 4 and 35 mm, corresponding to Reynolds numbers of 100 and 1000, respectively. The authors observed that two close-packed vortices were shed at the tail during the burst phase while the central flow directed away from the fish. However, because the effect of viscosity on larvae swimming was more substantial, the vortices created by the larvae were relatively wider and have lower vortex circulation than those created by the adults. In addition, during the coasting phase, the dominance of viscosity over inertia caused large vortical flows in the vicinity of the larva's body, and high vorticity resulted in severe reduction in the coasting distance, which significantly impaired the larva's swimming efficiency, that is, the zebra danio larvae swam in burst-and-coast mode with a considerably higher cost than their adult counterparts.

10
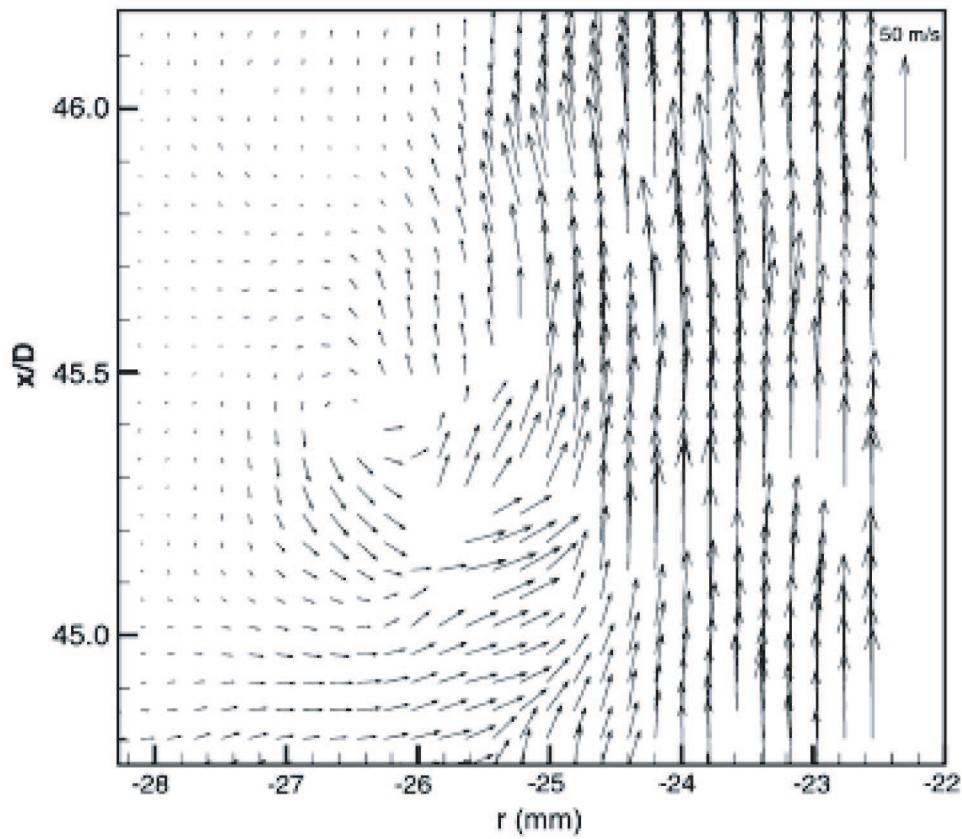
Figure 2.6. An example of instantaneous velocity vector maps taken at 0.13 second after ignition showing entrainment of surrounding gases by the emerging hot jet in the exhaust of a solid rocket motor (**?**).

Hanke et al. (2000) studied decay of the low-frequency water disturbances caused by swimming goldfish (60 and 100 mm body length) and found that the disturbances partially propagated as vortex-ring-like structures, leaving a hydrodynamic trail (wake) in the water that other animals, such as their predators, could pick up to determine the fish's presence even several minutes after the fish swam by.

Muller et al. (2001) investigated how the body contributes to the wake in undulatory fish swimming by measuring the flow fields around a swimming eel, which produces thrust by passing a transverse wave down its body. They found that the maximum flow velocities around the eel's body increased approximately linearly along the body from head to tail, which supports the hypothesis that eels generate thrust employing their whole body. In addition, the shape of the wake was very different from the optimized wake for maximum swimming efficiency or thrust, and instead, was suited for high maneuverability.

To evaluate fish swimming performance and examine the energetic balance of fish propulsion, it is imperative to quantify the hydrodynamic forces exerted on fish. An experimental simulation of the thrust phase of a fast-start swimming fish was conducted by Ahlborn et al. (1997) to directly measure thrust and accumulated impulse generated by a tail simulator. However, to date
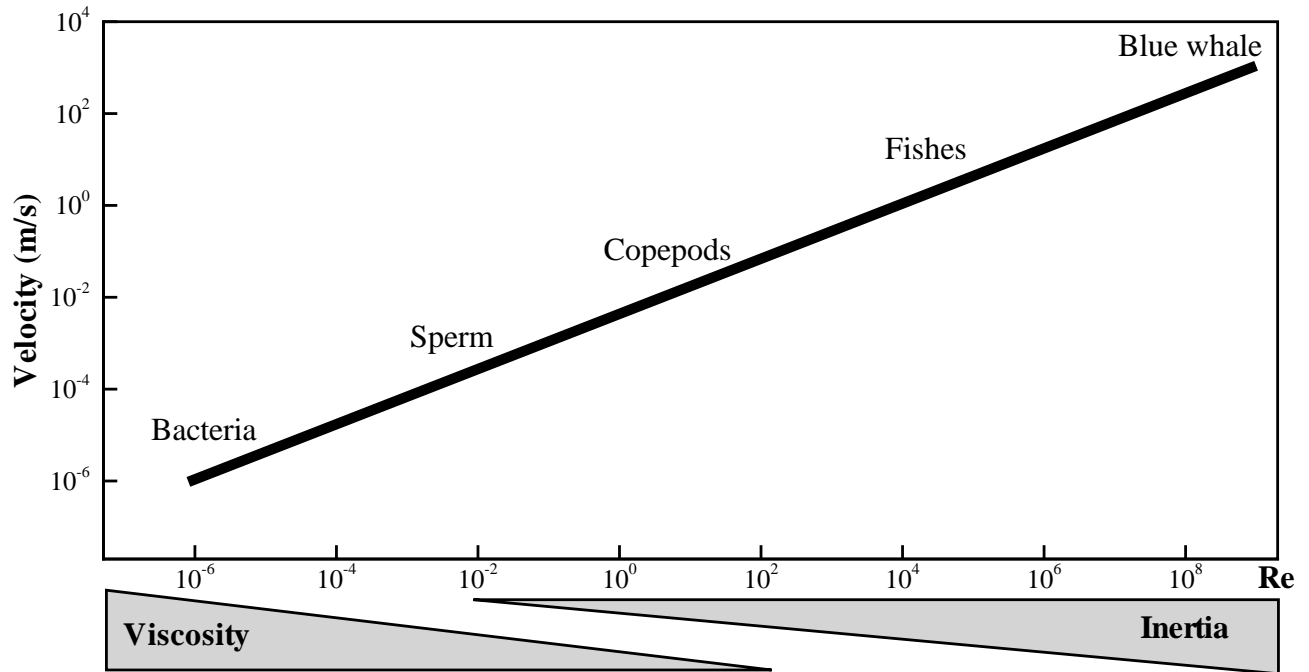
Figure 2.7. Animal swimming velocity versus Re number. The bar below the x-axis indicates the dominant flow regimes. Adapted from Videler (1993).

direct measurement of the hydrodynamic forces experienced by fish still poses a significant challenge. As a result, many theoretical and empirical models have been proposed, such as drag-based or lift-based locomotive mechanisms for steady swimming animals by Webb (1988) and the unsteady clap-and-fling mechanism by Lighthill (1973). Recently, to complement the experimental studies, computational approaches solving the unsteady Navier-Stokes equations have advanced considerably, such as computational fluid dynamics simulation of hawkmoth hovering and tadpole swimming by Liu et al. (1997) and Liu et al. (1998), simulation of bird wrasses with oscillating fins by Ramamurti et al. (2002), and simulation of tuna and giant danio by Zhu et al. (2002).

With particle image velocimetry, it is possible to map the instantaneous flow field adjacent to fish, visualize the downstream vortex structures, and ultimately calculate the forces experienced by the swimming fish. Drucker and Lauder (1999) investigated the feasibility of this methodology. They employed PIV to separately measure in three orthogonal planes the flow field in the wake of pectoral fins of bluegill sunfish swimming freely at speeds of 0.5–1.5 L/second, where the body length L was approximately 203 mm. Because the measurements in the three planes were not simultaneous, they used several fish to establish the general flow patterns, reconstruct the three-dimensional vortex structures, and obtain the forces in three dimensions from the vortex ring orientation and momentum. They found that the locomotive forces produced by the pectoral fins agree very well with empirically determined counter-forces of body drag and weight. They concluded PIV can measure accurately the large-scale vorticity in the wake of the freely swimming fish and is a very valuable tool for the study of unsteady animal-generated flows. They investigated the three-dimensional structure and strength of the wake of black surfperch to estimate the hydrodynamic forces (Drucker and Lauder 2000) and compared results with those experienced by the bluegill sunfish in the previous study (Drucker and Lauder 1999), with the objective of understand-

ing why some fishes are able to swim faster than others from a hydrodynamic perspective. In the wake of black surfperch, there are a pair of distinct vortex rings linked ventrally for all swimming speeds while there is one vortex ring per fin in the wake of bluegill sunfish at low speeds and a pair of linked vortex rings at high speeds. When the swimming speed increases, black surfperch orient the vortices to downstream directions more favorable to produce thrust. In contrast, bluegill sunfish generate relatively large lateral forces with paired fins. Therefore, black surfperch are able to swim much faster than bluegill sunfish. The authors also proposed two hypotheses: 1) at low swimming speeds it is necessary for both black surfperch and bluegill sunfish to generate large lateral forces to maintain stability, and 2) there is a potential trade-off hydrodynamically between speed and maneuverability, which is directly related to the lateral forces. The latter hypothesis leads to their argument that bluegill sunfish may be more maneuverable due to their ability to produce large lateral forces with the asymmetries of two paired fins, which were further studied by examining the details of the vortex structure in two subsequent studies (Drucker and Lauder, 2001a and 2001b). Details about how the caudal fin functions during locomotion, such as kinematics, flow visualizations, and evolutionary patterns, can be found in the review by Lauder (2000).

Nauen and Lauder (2002a) examined the performance of chub mackerel (200-260 mm body length, L) swimming steadily in a recirculating flow tank at cruising speeds of 1.2 and 2.2 L/s. By measuring the wake of the fish in the horizontal plane and vertical plane separately, the authors characterized quantitatively the vortex structure of the wake and obtained the lift, thrust, and lateral forces from the wake measurements. They noted that the wake consisted of a series of linked elliptical vortex rings, with the length of the minor axis of the vortex rings about the size of the caudal fin span and the length of the major axis dependent on the magnitude of the swimming speed. The authors also performed drag measurements by towing the same fish post mortem and compared the results with the thrust estimates from the PIV experiments, concluding that the two thrust measurements were not significantly different. In addition, they reported that there was no change in lift production with increased swimming speeds, while the lateral force generation increased considerably.

Nauen and Lauder (2002b) applied stereoscopic digital particle image velocimetry (stereo-DPIV) to study the wakes in three dimensions for freely swimming rainbow trout (*Oncorhynchus mykiss*). Previous PIV studies of animal-generated flows were generally two-dimensional, typically in horizontal (frontal) or vertical (parasagittal) plane. Reconstruction of three-dimensional flow visualization from separate two-dimensional measurements requires combination of a series of measurements of repetitive behavior in orthogonal planes (Drucker and Lauder 1999). By comparing their direct three-dimensional results with those obtained via the combination of two-dimensional measurements, the authors demonstrated the feasibility of employing stereo-PIV to study freely swimming fish, and pointed out the advantage of stereo-PIV for simultaneously three-dimensional flow visualization of non-repetitive, highly variable behaviors.

Besides from the visualization of the vortex structure in the wake of the fish, thrust and other forces can also be obtained from the boundary layer around the fish body. As an object moves through a fluid, or as a fluid moves past an object, a boundary layer is created due to viscosity as a thin layer of fluid near the surface in which the velocity changes from zero at the surface to the free stream value away from the surface (Batchelor 1967). However, because of the motion of its body, the boundary layer of a swimming fish is more complicated than that of a rigid body, such as an aerodynamic wing, which can be tested in a wind or water tunnel. In addition, the complication

is further enhanced by the coupling of the thrust-generation and drag-generation mechanisms for a swimming fish. As a result, there are many discrepancies between the drag predictions by various investigators.

To examine the differences of the various drag prediction theories for freely swimming fish, Anderson et al. (2001) measured the tangential and normal velocity profiles of the boundary layers surrounding two freely swimming fish: carangiform swimming scup (195 mm body length) and anguilliform swimming dogfish (444 mm body length), with the Reynolds number ranging from 3×10^3 to 3×10^5. The scup was tested in both still water and a flume, and the dogfish was observed swimming in the flume only. They found that in still water, the boundary layer was always laminar due to relatively low Reynolds numbers, and in the flume, the boundary layer became turbulent as the Reynolds number increased. No separation of the boundary layer was reported and the profiles agreed well with the classic laminar and turbulent boundary profiles such as Blasius, Falkner and Skan, and the law of the wall, but the behavior of local friction coefficients, boundary layer thickness, and fluid velocities were very different from the behavior of those variables in the boundary layer of a rigid body. Furthermore, the friction drag experienced by the swimming fish was much higher than the rigid-body friction drag.

Besides the studies of the thrust-production and drag-reduction mechanisms of freely swimming fish, it is also very interesting and important to understand how fish adapt to or exploit environmental turbulence to reduce locomotive cost and improve swimming efficiency. Liao et al. (2003a, 2003b) investigated how rainbow trout (100 mm body length, L) voluntarily altered their body in Kármán vortex street. Two swimming speeds, 2.5 and 4.5 L/s were tested in the Kármán vortex streets created by two different diameter cylinders, 25 and 50 mm. They reported that the trout swimming behind the cylinders adopted a unique pattern of axial body movement to hold station, which was termed Kármán gait by the authors. They proposed that trout employed Kármán gait to reduce locomotive costs by modifying their body kinematics and absorb energy from the vortices in the low-pressure, high-vorticity regions behind the cylinders, instead of taking advantage of the reduced flow velocity. They suggested that the occurrence of Kármán gait depended on the hydrodynamic stability and strength of the cylinder wake. Kármán gait could be triggered more easily with relatively stable vortex street and only certain range of flow velocities and cylinder sizes could produce periodic and stable vortex-shedding to induce a regular kinematic response.

In summary, almost all previous PIV studies of fish focused on the performance evaluation of freely swimming fish and very few investigated the fish injury mechanisms due to the challenging features of the flow structures and limitation of the regular PIV technique. Usually the time scales for fish-structure interaction are only a fraction of a second, and regular PIV technique has a sampling rate ranging from 10 to 30 Hz.

In addition, the majority of previous investigations dealt with the lower end of the Reynolds number range. The fish of our interest, such as rainbow trout and spring and fall Chinook salmon, fall into the middle range, in which neither viscosity nor inertia is negligible, and three-dimensionality has yet to dominate.

3.0 PNNL Test of Feasibility of Applying High-Speed PIV to Flow Around Fish

Based on the literature review in Chapter 2, previous PIV studies of fish focused on freely swimming fish instead of fish injury mechanisms due to the limitation of regular PIV technique and complexity of turbine environments. In addition, the Reynolds number range of our interest falls outside of the range of the existing literature.

The recent development of high-speed PIV made possible better understanding of the biological responses of juvenile fish in turbulent hydraulic environments. In late 2003 and 2004 Pacific Northwest National Laboratory evaluated the feasibility of applying high-Speed PIV to fish injury studies.

3.1 Methods

3.1.1 Experimental Setup

A two-dimensional digital particle image velocimetry system from Oxford Laser Inc. was used in this study. The flow was illuminated by a LDP diode-pumped Nd:YAG pulsed laser which has the capability of producing average power of 15 watts at 532 nm at a repetition of 1,000 Hz and has a pulse width of 60 ns. The laser beam was spread using a negative cylindrical lens into a sheet of 220 mm in the *x–y* measurement plane and the sheet was focused with a positive spherical lens to a waist near the middle point of the test section. Its greatest thickness in the field of view of 220 mm $\times$ 220 mm was roughly 0.8 mm.

Seeding particles were 70-micron glass spheres with a density of 1.18 g/cm^3. The scattered light of the tracer particles was imaged into a Photron 1280 PCI high-speed, high-resolution digital camera. The camera employs a 10-bit CMOS sensor with global electronic shutter as fast as 7.8 μs. It is capable of a 500 frame-per-second frame rate at a resolution of 1280 x 1024 pixels and up to 16,000 frame-per-second at reduced resolutions.

The timing of the laser pulses and the CCD camera was controlled by a synchronizer. A schematic of the optical configuration is included in Figure 3.1. Because a pair of images are needed to produce a velocity vector field, a sampling rate of 500 Hz was used in the current study with the camera operating at 1,000 frame-per-second.

Photron PFV V2.0 software was used for image acquisition. The double-exposed images were then interrogated using double-frame cross-correlation. The interrogation was performed using VidPIV V4.0 software. The size of interrogation spots was 16 pixels $\times$ 16 pixels, which corresponds to a spatial resolution of 1.5 mm $\times$ 1.5 mm.

A round water jet was submerged into an aquarian tank to create a quantifiable shear environ-
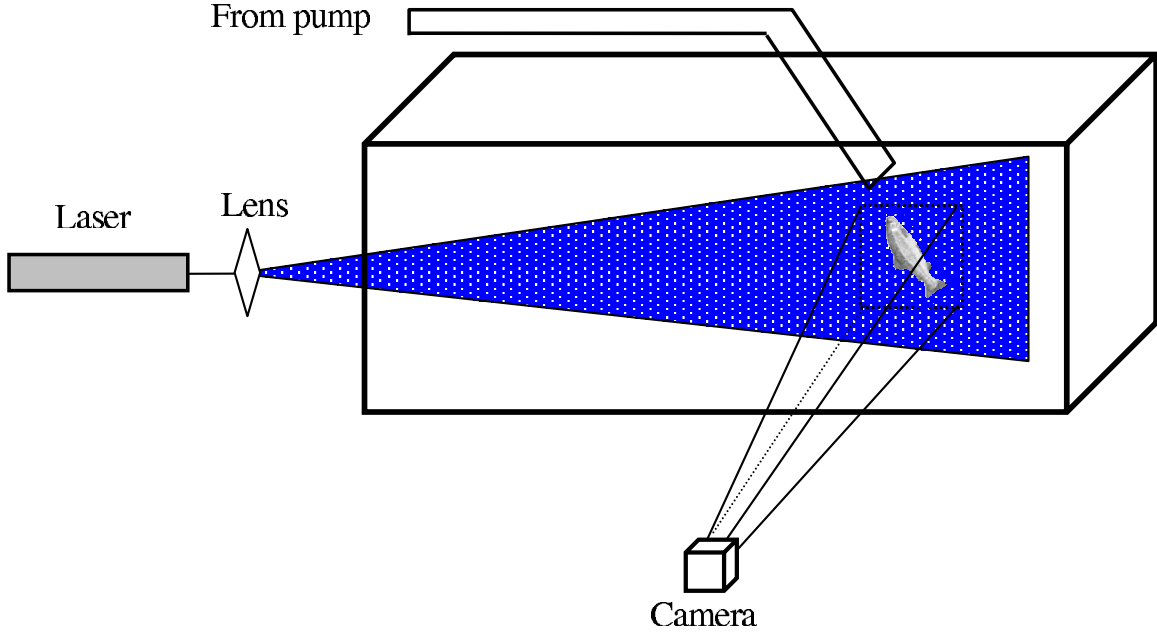
Figure 3.1. Schematic of experimental setup.

ment. The tank was 3 m × 0.9 m × 0.9 m, and the jet was 0.038 m in diameter.

3.1.2   Calculations of Measurement Errors

Prasad et al. (1992) showed that, when particle images are well-resolved during digitization, the random error associated with particle displacement estimation in PIV using a simple cross-correlation method is approximately five percent of the particle image diameter. In the current study, the particle images were roughly two pixels in diameter, so the root-mean-square random error was about 0.1 pixels. Furthermore, since the maximum particle displacements in the PIV measurements were ten pixels, the relative uncertainty in the PIV measurement of a single instantaneous velocity vector due to error in measuring displacement was approximately one percent of the full-scale velocity. These random errors averaged to zero. There were also bias errors in PIV that do not average to zero. These were estimated to be less than one percent of the full-scale velocity (Liu et al. 1991).

As we discussed in Section 2.1, because PIV measures Eulerian flow field by computing the Lagrangian velocities of the seeding particles, it is essential that the seeding particles follow the flow faithfully. For a single particle in a dilute suspension of a Newtonian fluid, we assume that the effects of added mass, unsteady drag forces, non-uniform fluid motion, and pressure gradient are negligible (Adrian 1991), then the equation of motion is simplified as

$$\rho_P \frac{\pi d_p{}^2}{6} \frac{d\mathbf{v}}{dt} = C_D \frac{\rho \pi d_p{}^2}{8} (\mathbf{v} - \mathbf{u})|\mathbf{v} - \mathbf{u}| \tag{3.1}$$

where ρ_p and d_p are the density and the diameter of the particle, respectively; C_D is the drag coefficient; $\mathbf{v}$ and $\mathbf{u}$ are the velocities of the particle and the fluid, respectively, and $\mathbf{v} - \mathbf{u}$ is the slip velocity of the particle.

16

From equation (3.1), the magnitude of the slip velocity can be obtained

$$|\mathbf{v} - \mathbf{u}| = \sqrt{\frac{4\rho_p\, d_p}{3\rho C_D} |\frac{d\mathbf{v}}{dt}|} \qquad (3.2)$$

Suppose the Reynolds number based on the velocity and and the diameter of the particle is small, i.e., $\frac{\rho|\mathbf{v}-\mathbf{u}|d_p}{\mu} \ll 1$, and apply Stoke's law for the evaluation of the drag coefficient (Batchelor 1967)

$$C_D = \frac{24\mu}{\rho d_p |\mathbf{v} - \mathbf{u}|} \qquad (3.3)$$

where μ is the dynamic viscosity of the fluid.

Substituting equation (3.3) into equation (3.2) yields

$$|\mathbf{v} - \mathbf{u}| = \frac{\rho_p\, d_p^2}{18\mu} |\frac{d\mathbf{v}}{dt}| \qquad (3.4)$$

For the current experimental setup, suppose the particle velocity is about 1 m/s, the flow velocity has a change of 1 m/s over a distance of 0.01 m, which corresponds to an acceleration of approximately 100 m/s^2, and the particle density and diameter are 1.1 g/cm^3 and 10 μm, then the slip velocity predicted by equation (3.4) is 0.00055 m/s, which is about 0.055% of the flow velocity. This confirms that PIV measurement errors due to particle slip are negligible, that is, the Lagrangian velocities of the seeding particles provide accurate representation of the Eulerian flow field.

3.1.3   Acquiring Measurements

Velocity measurements were acquired for the jet at an exit velocity of 2.2 m/s. The corresponding Reynolds number is 8.4×10^4, well above the minimum of 4000 to achieve fully developed turbulence according to Fischer et al. (1979). The contours and vector map of the whole field are plotted in Figures. 3.2 and 3.3.

A rainbow trout (*Oncorhynchus mykiss* , 108 mm body length) was held in the jet, with the tail towards the nozzle. One thousand instantaneous velocity fields were acquired for both the flow field around the whole fish and zoomed-in area around the head. Mean velocity fields, instantaneous vorticity fields, and instantaneous exposure strain rate fields were then computed from the instantaneous velocity measurements.

3.2   Results and Discussion

Figures 3.4 to 3.6 show contour plots of the mean velocity, mean vorticity, and mean exposure strain rate of the flow in the vicinity of the fish, and Figures 3.7 and 3.8 show contour plots of an instantaneous velocity, related vorticity, and related exposure strain rate of the flow in the vicinity of the fish. The contour plots of vorticity fields are overlapped with the velocity vectors to better
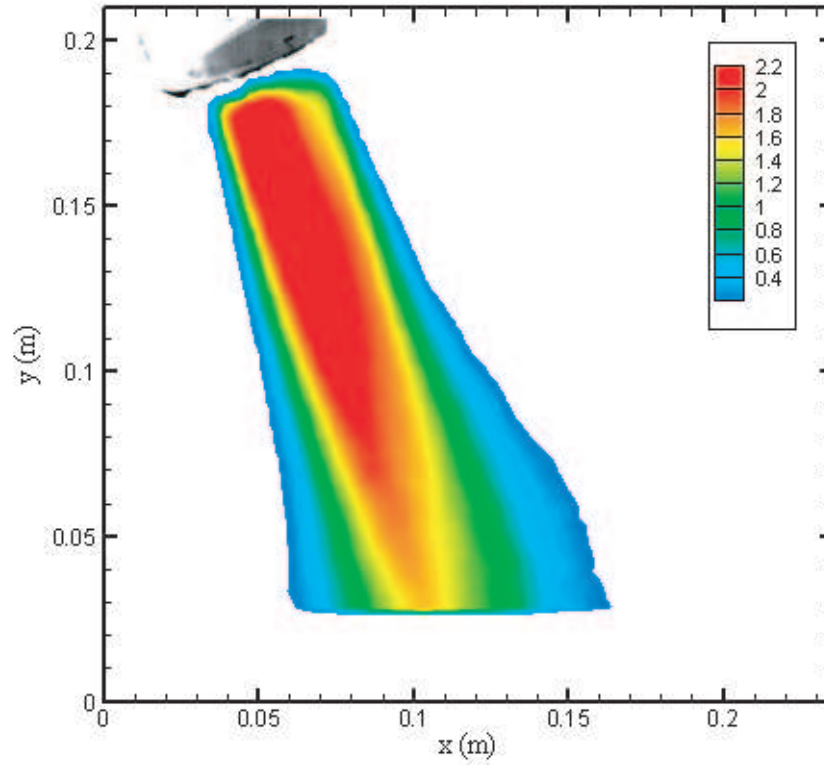
Figure 3.2. Contour plot of mean velocity field of Jet (in m/s).
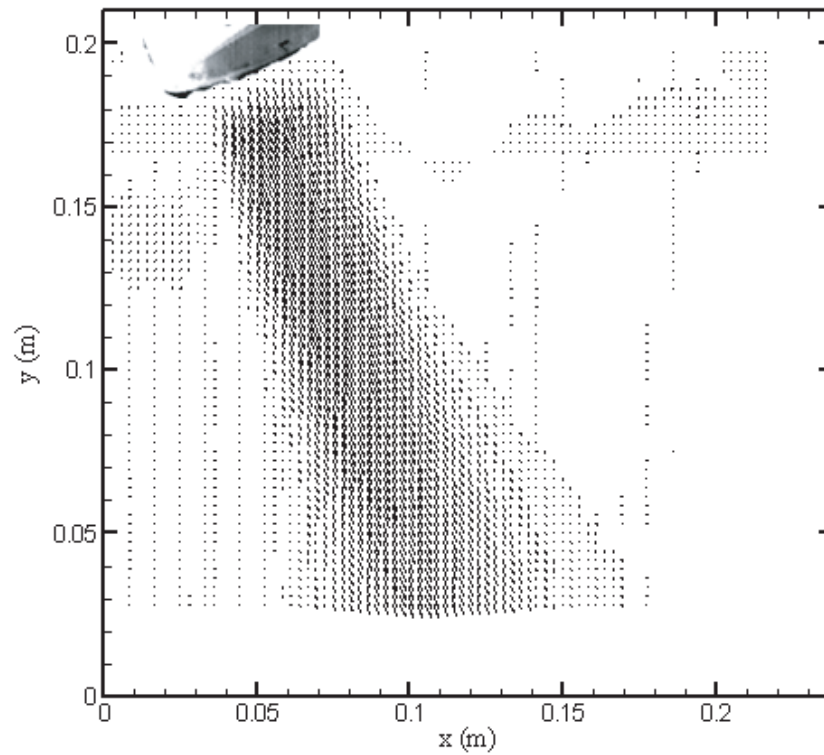
Figure 3.3. Vector plot of mean velocity field of Jet.
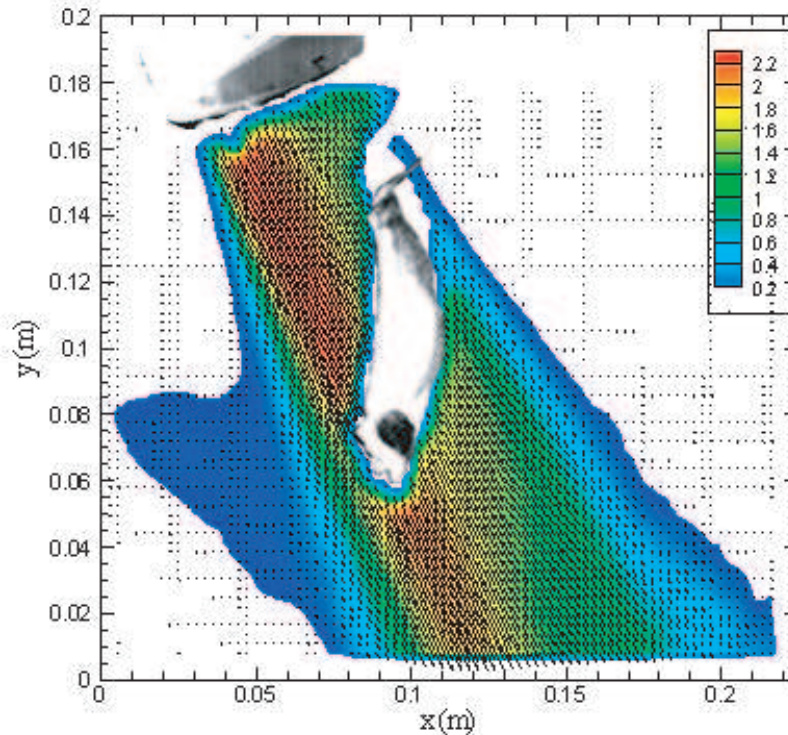
Figure 3.4. Mean velocity field around fish held in a water jet (in m/s).

visualize the vortical structures. For both mean and instantaneous vorticity fields, there is very strong vorticity over the fish back facing the jet, which confirms the steady feature of vortical structure and complexity of the boundary layer over the body. However, in the instantaneous vorticity field (Figure 3.7), there are a series of small-scale vortices, which are not present in the mean vorticity field (Figure 3.5). This indicates that in the wake of the fish, vortex-shedding is unsteady. This unsteady behavior is further substantiated by the contour plots of exposure strain rate. As shown in Figures 3.6 and 3.8, besides large shear stresses in regions adjacent to the body, in the wake there are a sequence of large stress spots indicating vortices in the instantaneous flow field; in contrast, the vortices are averaged out in the mean flow field, indicating the unsteady feature of the vortex-shedding in the wake.

Measurements were also taken in the immediate vicinity of the fish head to obtain more detailed information about the effects of the flow on fish. Figures 3.9, 3.10 and 3.11 show the mean velocity, mean vorticity, and mean exposure strain rate fields, respectively; while Figures 3.9, 3.10 and 3.11 describe the corresponding instantaneous velocity and vorticity, and instantaneous exposure strain rate fields, respectively. Velocity vectors are overlapped with the vorticity contours for better visualization of the vortical structures.

Consistent with previous observations, in both the mean and instantaneous fields, very high vorticity and exposure strain rate occur around the fish head, with the highest in the pectoral area as shown in Figure 3.11. This evidence supports the conclusions made by Neitzel et al. (2000) and Deng et al. (2004a) that the operculum are most vulnerable to damage from the turbulent shear flow, because they are easily pried open, essentially capturing the energy contained in a

19
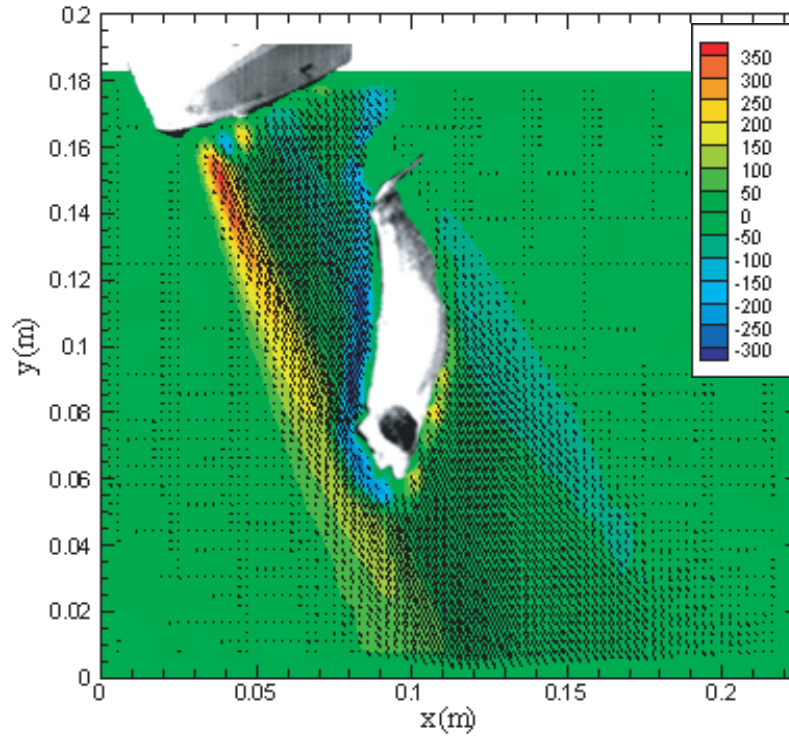
Figure 3.5. Contour plot of mean vorticity field around fish held in a water jet (in $\frac{m/s}{m}$).
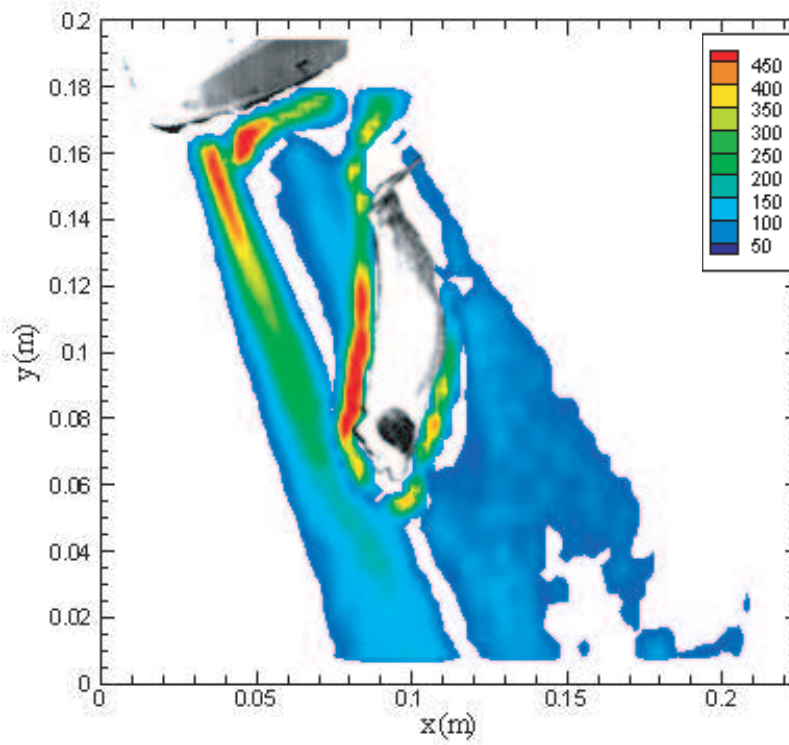
Figure 3.6. Contour plot of mean exposure strain rate field around fish held in a water jet (in $\frac{m/s}{m}$).
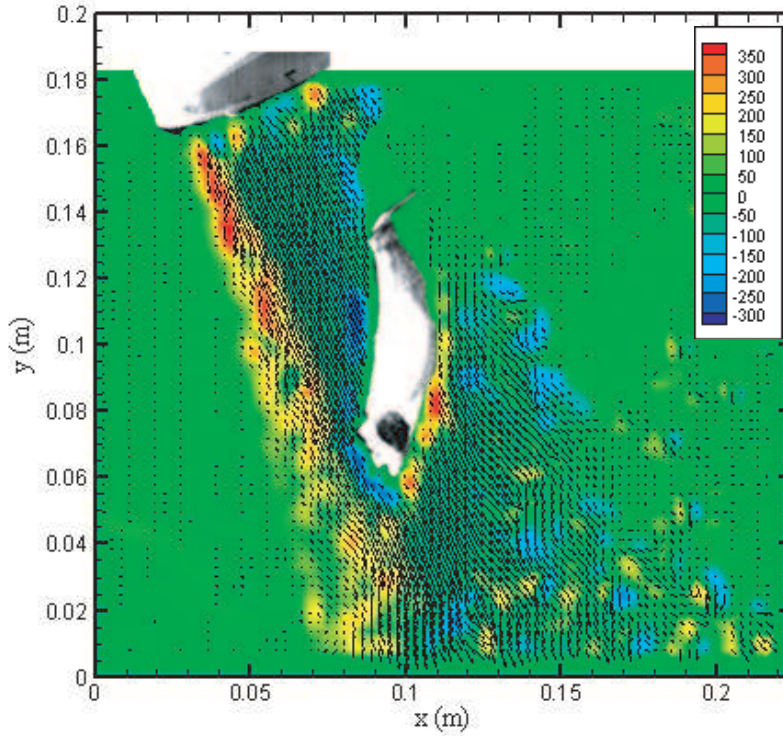
Figure 3.7. Contour plot of instantaneous vorticity field around fish held in a water jet (in $\frac{m/s}{m}$), overlapped with instantaneous velocity vectors.

Figure 3.8. Contour plot of instantaneous exposure strain rate field around fish held in a water jet (in $\frac{m/s}{m}$).
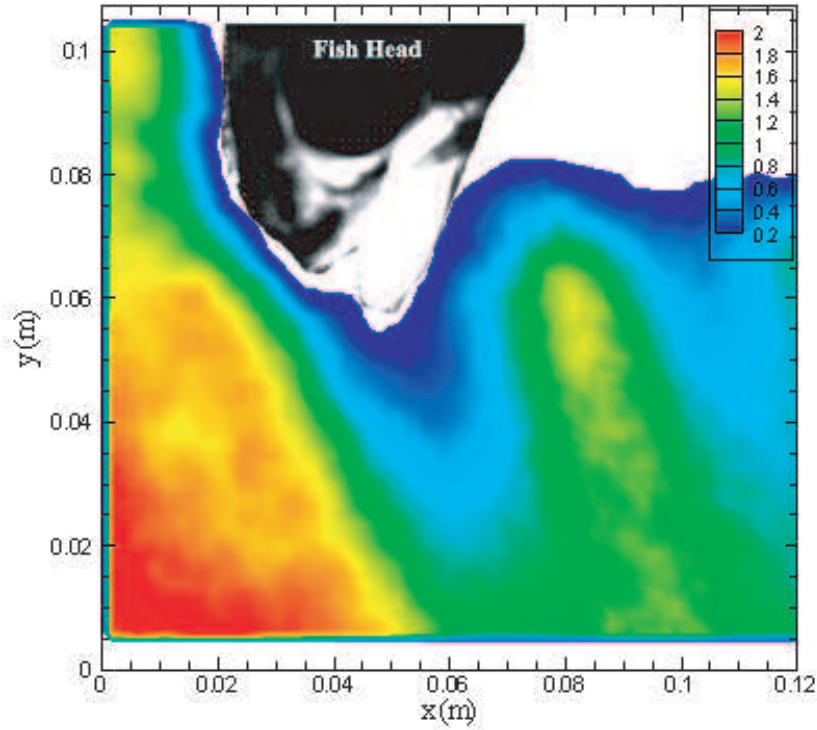
Figure 3.9. Contour plot of mean velocity field around fish head held in a water jet (in m/s).

disproportionately large area of high flow; besides, the large vorticity and shear stress can lift and tear off scales, rupture or dislodge eyes, and damage gills.

In addition, the zoomed-in region also demonstrates the unsteady behavior of the vortex-shedding in the wake, which implies that injury to fish by the instantaneous flow structures would likely be much higher. Three movies (velocity_head.avi, vorticity_head.avi, stress_head.avi) are attached to show the instantaneous features of velocity, vorticity, and exposure strain rate, respectively.

Figure 3.10. Contour plot of mean vorticity field around fish head held in a water jet (in $\frac{m/s}{m}$).

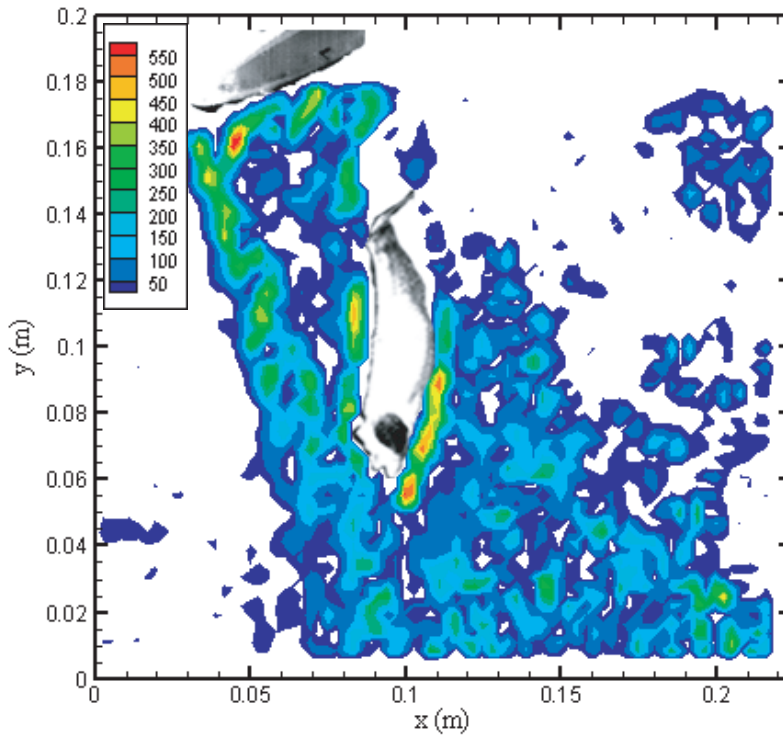**Figure 3.11.** Contour plot of mean exposure strain rate field around fish head held in a water jet (in $\frac{m/s}{m}$).
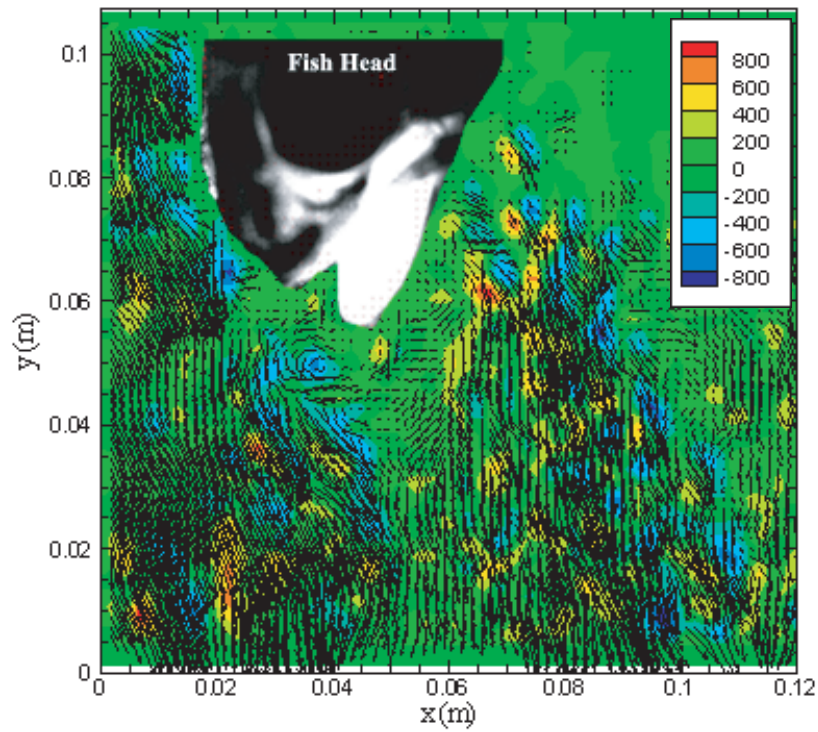
Figure 3.12. Contour plot of instantaneous vorticity field around fish head held in a water jet (in $\frac{m/s}{m}$), overlapped with instantaneous velocity vectors.
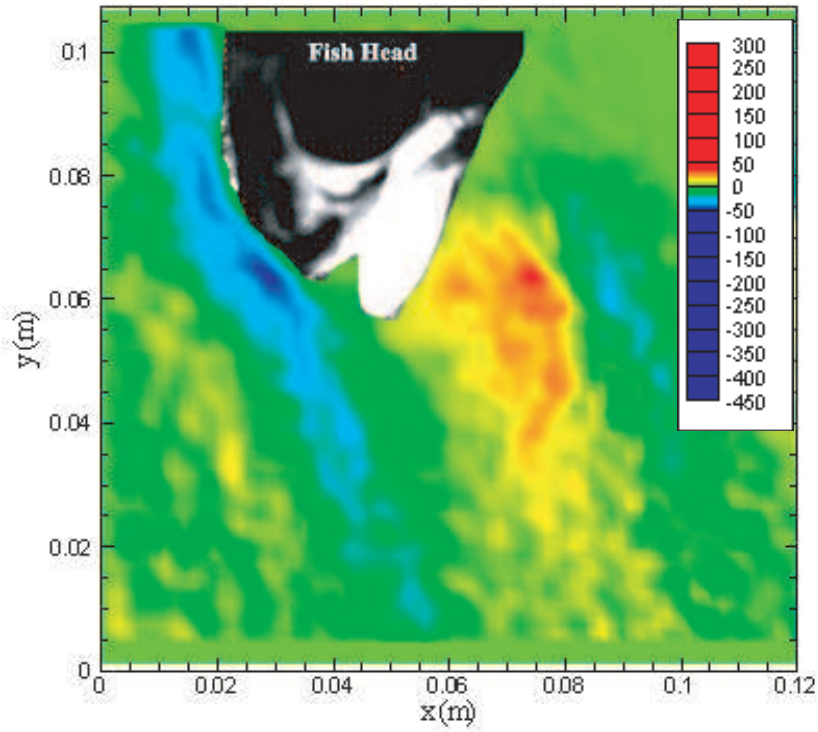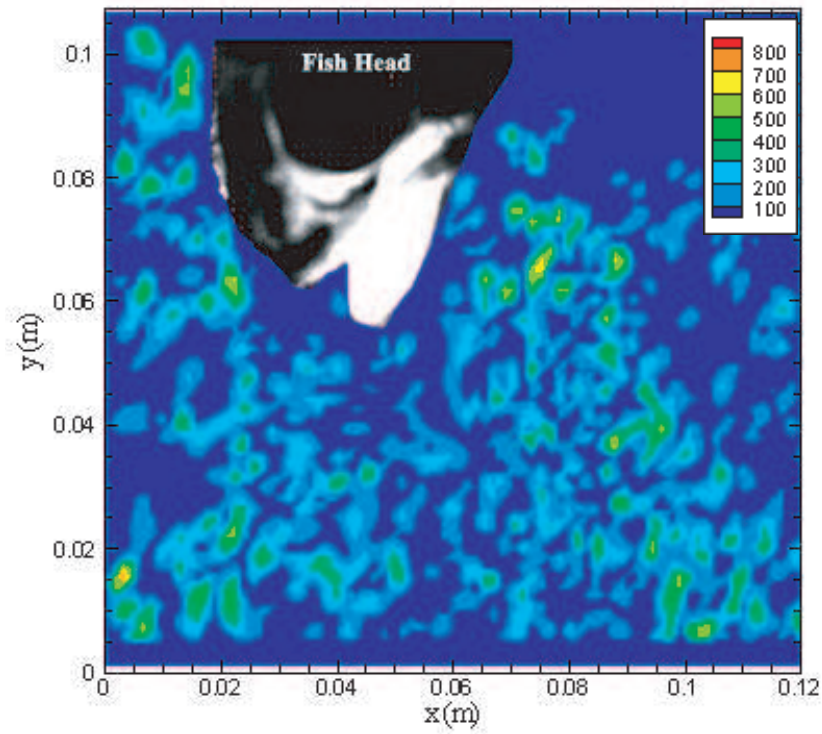
Figure 3.13. Contour plot of instantaneous exposure strain rate field around fish head held in a water jet (in $\frac{m/s}{m}$).
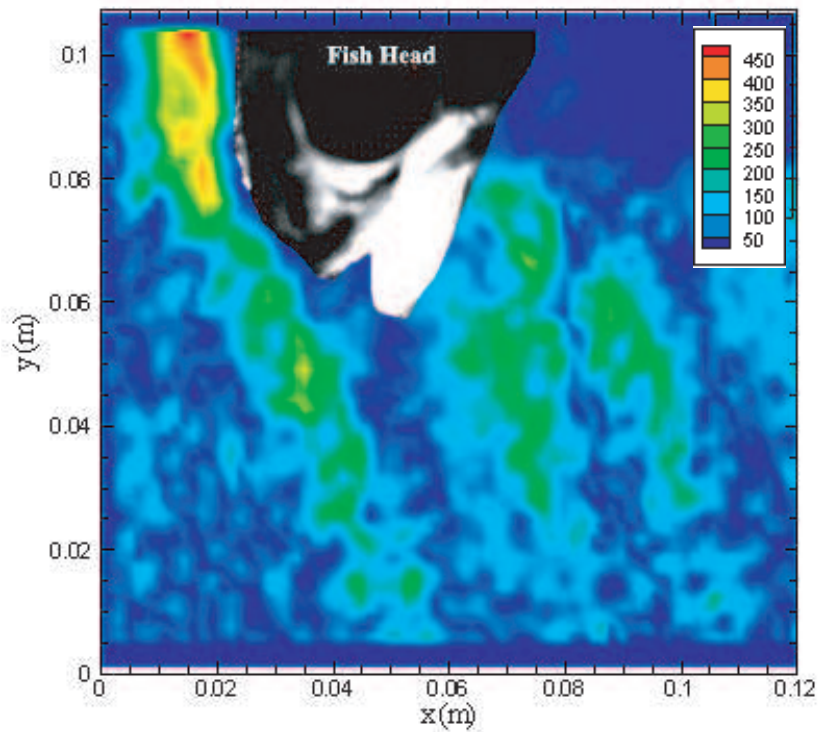
4.0 High-Speed, High-Resolution Digital Imaging and Advanced Motion Analysis

Motion-tracking from video data is becoming a common experimental tool. Numerous researchers have used video data to study various aspects of swimming fish or their reactions (Liao and Lauder 2000; Tang et al. 2000; Hughes and Kelly 1996). However, these swimming studies typically do not require exceptionally high camera frame rates. High-speed (500-1,000 frame-per-second) video studies of fish tests, especially injury experiments, are less common. Some common high-speed applications of motion tracking analysis include crash testing in the auto industry (Kang et al. 2001) and studies of impacts and projectile motion (Tanaka et al. 2002; Hrubes 2001). Two objectives for this part of this study were to use high-speed high-resolution digital cameras and advanced motion analysis technique to better quantify the kinematic and dynamic parameters associated with the exposure of fish or Sensor Fish to turbulent shear flow, and the accuracy of bead tracking (emulating fish in prototype) in physical models. The kinematic parameters included the velocity ($\mathbf{v}$), acceleration ($\mathbf{a}$), jerk ($\mathbf{J}$), and bending angle (θ_b) of the body, while the dynamic parameter was the bulk force (F) on the object. The injury type and severity were then related to fish size (length and mass), exposure strain rate, and magnitude of kinematic and dynamic parameters computed from video-derived 3-D trajectory paths.

4.1 Experimental Methods

4.1.1 Test Facility

A rectangular flume containing a submerged water jet was used to create a quantifiable shear environment consistent with conditions expected within a hydroelectric turbine. The flume was 9 m long by 1.2 m wide by 1.2 m deep when filled with water. A conical stainless-steel nozzle that began at 25.4 cm diameter and constricted to a circular 6.35 cm diameter over 50.8 cm in length was bolted to a flange inside the flume. This nozzle configuration provided a contraction ratio of 5:1 that effectively accelerated flow and reduced non-uniformity in the inlet velocity distribution. Viewing windows are located on the side and bottom at the nozzle end of the flume to record fish reactions as they enter test flow fields. A flow conditioner was incorporated upstream of the nozzle. More details about the test facility can be found in Neitzel et al. (2000, 2004).

Fish and Sensor Fish were actively introduced into the jet through a 60 cm long x 3.18 cm diameter polycarbonate introduction tube with a velocity of 0.81 m/s. The tube was fastened above the nozzle at an angle of 30 (Figure 4.1). The terminus of the introduction tube was positioned above and in front of the terminus of the nozzle, with only a 1-cm vertical gap to ensure that test fish contacted the jet. The introduction flow was necessary to ensure that fish passed the terminus of the introduction tube smoothly.
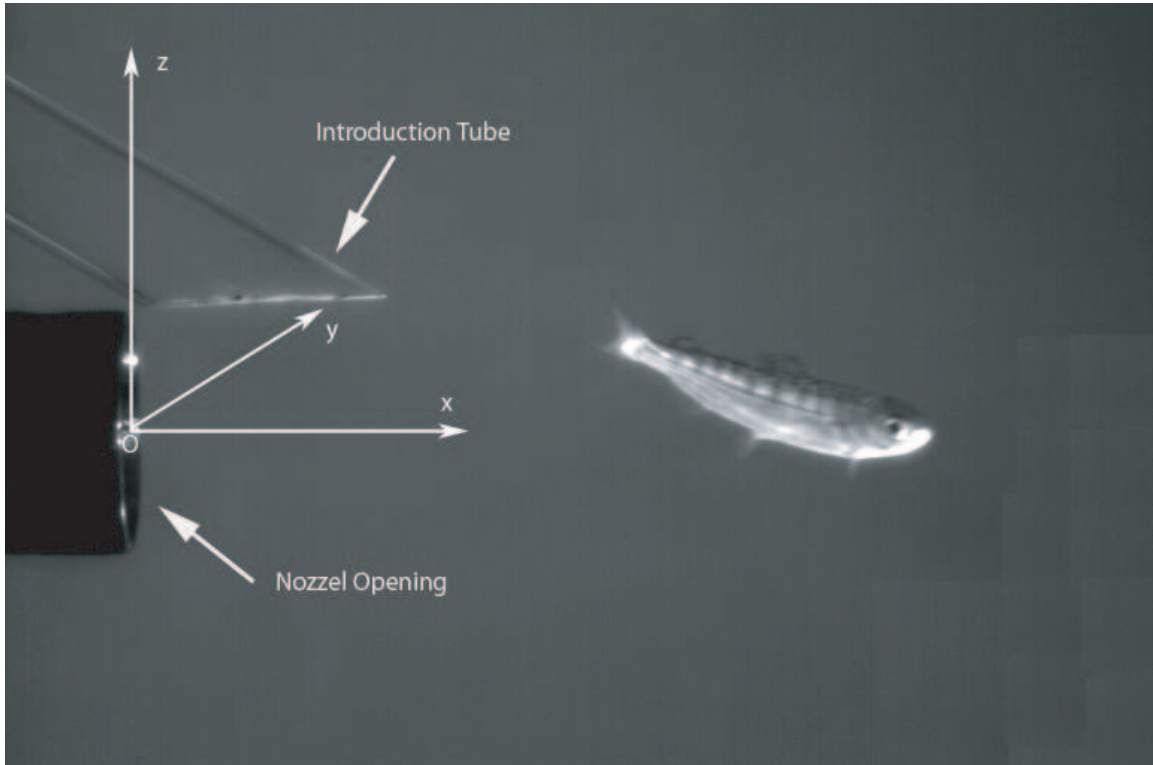
Figure 4.1. Nozzle, introduction tube, coordinate system, and a test fish being released.

4.1.2   High-Speed Camera

Digital video images of exposed fish, Sensor Fish devices, and beads were captured using two identical high-speed digital cameras (Photron PCI FastCAM 1280) equipped with 50-mm lenses. The cameras captured side (X-Y plane) and bottom (X-Z plane) views through polycarbonate viewing windows in the side and bottom of the tank. Halogen lamps were used to provide the desired illumination and a gray-colored back panel was used to provide optimal contrast. The cameras recorded fish orientation and location from the moment a fish descended the introduction tube and contacted the shear environment, until it was swept out of the immediate shear environment (0.5 m) downstream. An entire exposure sequence lasted only a fraction of a second. Cameras recorded each event simultaneously at 1000 frames-per-second, which provided an approximate two seconds buffer of stored memory. Cameras were focused using a high-contrast resolution target positioned along the axis of the nozzle. Calibration of the field of view was accomplished by using the outer diameter of the nozzle.

4.1.3   Fish and Sensor Fish

The test fish were subyearling fall chinook salmon (Oncorhynchus tshawythscha) from stocks originating at the Priest Rapids Hatchery in Washington State. The fish size ranged from 93 to 128 mm in length and 8.1 to 23.5 grams in mass.

The Sensor Fish device was also tested in the same facility. Since its field trials in 1999,

Figure 4.2. A three degree-of-freedom Sensor Fish wrapped with black tape and marked with white stickers.

the Sensor Fish device has been an important tool to characterize the exposure conditions that fish experience during turbine, spillway, and other hydraulic environments (Carlson et al. 2003; Carlson and Duncan 2003). To better track the motion of Sensor Fish, we wrapped them with black tape and stuck white stickers around the body, as shown in Figure 4.2. A pair of snapshots of Sensor Fish captured by the two cameras is included in Figure 4.3.

4.1.4   Beads

The beads used in the current investigation were yellow, oblong, and slightly negatively buoyant. The size and density of one bead were approximately 4.28 mm × 3.28 mm × 2.23 mm, and $1.072 \times 10^3 \ kg/m^3$, respectively, which is comparable to the length of the fish used in live fish tests. The density also would be similar to that of a salmon smolt with mostly empty air bladder. Note that the beads were tested in the same flow facility as was used in the PIV experiments (Figure 3.1).

4.1.5   Motion analysis

VisualFusion (Boeing-SVS 2003) was used to analyze the 3-D motion of the fish/Sensor Fish and beads captured by the high-speed camera. This software is a powerful target tracking and motion analysis tool with many applications such as automotive crash testing, airbag deployment, missile flight analysis, and particle flow. It is specifically for analysis of target motion captured in a series of images. Analysis can be performed on a single image sequence obtained from one camera, in order to produce 2-D motion analysis, or analysis can be performed on multiple image sequences obtained from multiple cameras in order to produce 3-D motion analysis. Target motion includes not only (x,y,z) coordinates versus time, but also size, shape, orientation, and brightness parameters. Visual Fusion also has a number of image processing modules that were used to enhance or suppress different features in an image, allowing tracking of specific targets against complex backgrounds.
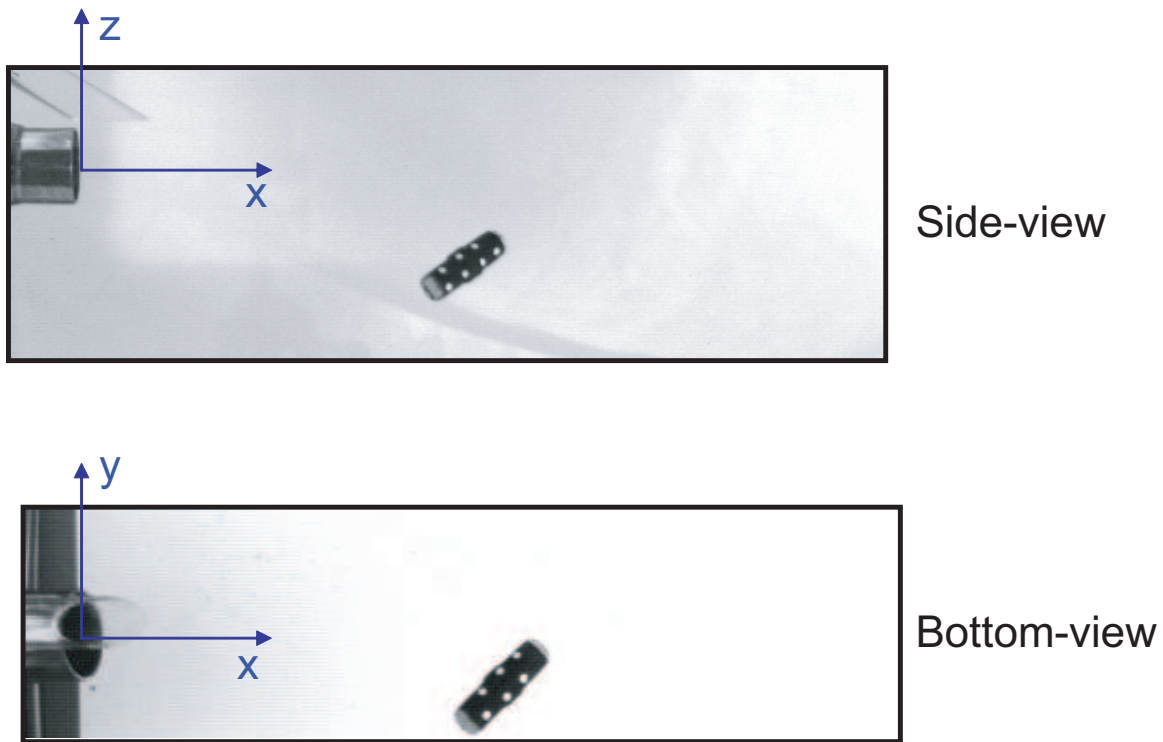
Figure 4.3. A pair of snapshots of Sensor Fish device captured by the two cameras.

For the image sequences in the current study, the target of an object was defined by specifying a threshold value based on the contrast (in brightness) between the pixel values of the object and the background. The centroid of the image of the object in a frame was used to represent the position of the object. A frame-to-frame correlation was performed in order to link the target locations of a specific object, and generate a track for the object. The 2-D trajectory (time history of displacement in engineering units) of the object was obtained by calibrating and referring back to the actual physical scales. In the current investigations, the two cameras were synchronized in operation, so the position versus time data for for each camera could be interpolated to a common time base. With the two simultaneous 2-D trajectories, an exact solution for 3-D trajectory was then found via 3-D triangulation. Refer to Boeing-SVS (2003) for details of mathematics.

For a known rigid body such as Sensor Fish, six-degree-of-freedom (6DOF) motion analysis can be performed by tracking four non-coplanar points in the body with a single camera. In general, a point on a 3D object located in space is projected onto the focal plane of a camera to form an image. The projection may be modelled as a full perspective projection for a distortion free lens (for a lens containing geometric distortion, a lens distortion correction can be applied to the lens to map observed object locations to their undistorted locations). With a mathematical model of the object and some camera parameters involved in the geometric projection, a 6DOF algorithm can be developed to invert the 3-D to 2-D projection process, to determine what 3-D position and orientation of the object would have generated the observed image. With the orientation of yaw, pitch, and roll in addition to the 3-D translational motion, this technique will greatly benefit the development and testing of the new 6DOF Sensor Fish (Deng et al. 2004b).

30

4.1.6 Kinematic and Dynamic Parameters

The kinematic and dynamic parameter time series were computed from the change in the x, y, z position of the centroid of the fish for each successive time step. Simplified expressions for each variable are shown in the equations below:

$$\mathbf{r} = x\,\mathbf{i} + y\,\mathbf{j} + z\,\mathbf{k} \tag{4.1}$$

$$\mathbf{v} = \frac{d\mathbf{r}}{dt} \tag{4.2}$$

$$\mathbf{a} = \frac{d\mathbf{v}}{dt} \tag{4.3}$$

$$\mathbf{F} = m\mathbf{a} \tag{4.4}$$

$$\mathbf{J} = \frac{d\mathbf{a}}{dt} \tag{4.5}$$

$$\theta_b = \arccos\left(\frac{A^2 + B^2 - C^2}{2AB}\right) \tag{4.6}$$

where $\mathbf{r}$ is the trajectory vector, $\mathbf{v}$ is the tracked velocity, $\mathbf{a}$ is the acceleration, $\mathbf{F}$ is the force, $\mathbf{J}$ is the jerk (rate of change of acceleration), m is the fish mass, and dt is the time step (equal to the time between digitized frames). The values A, B, and C are the three sides of a triangle formed by the bent fish, where A and B are the sides formed by the fish body and C is the side connecting the head and tail (opposite to θ_b).

4.2 Results for Fish and Sensor Fish

The trajectories of four separate points on each fish and Sensor Fish were tracked frame by frame using Visual Fusion 4.2. The side and bottom view tracks were then combined to form a 3-D trajectory, from which time series of the velocity, acceleration, jerk, bending, and force magnitudes were calculated. Two snapshots of the motion tracking process are shown in Figures 4.4 and 4.5. Two short clips of the tracking process are also included as .avi files on the compact disc attached with the report.

Only random errors associated with motion analysis were considered based on the assumption that the systematic errors were relatively small in comparison. To reduce random errors, the position data were smoothed with a 5-point boxcar average prior to the computation of higher-order parameters. Given an assumed maximum random error of one pixel in each direction associated with the motion analysis methodology, the related random errors for other parameters were then estimated. The related errors in percentage of full range of measurements for $|\mathbf{v}|$, $|\mathbf{a}|$, $|\mathbf{F}|$, and $|\mathbf{J}|$ are 1.6%, 7.1%, 7.2%, and 15.2%.

Motion analysis results of a fish release at a nozzle speed of 19.8 m/s are plotted in Figure 4.6 as an example to demonstrate the applicability of high-speed, high-resolution imaging with advanced motion analysis to the study of biological response of fish in hydraulic environments.

31
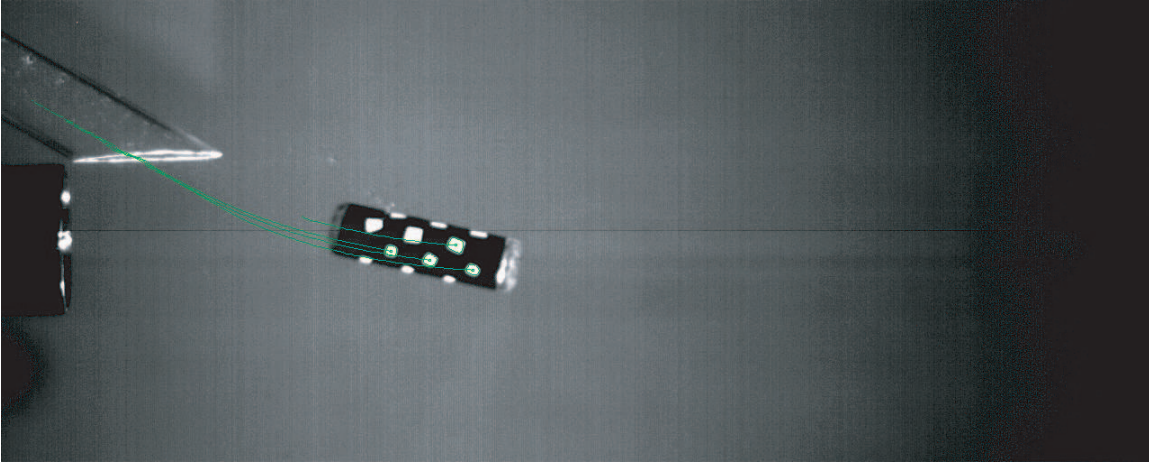
Figure 4.4. A snapshot of motion tracking of Sensor Fish in a turbulent shear flow.
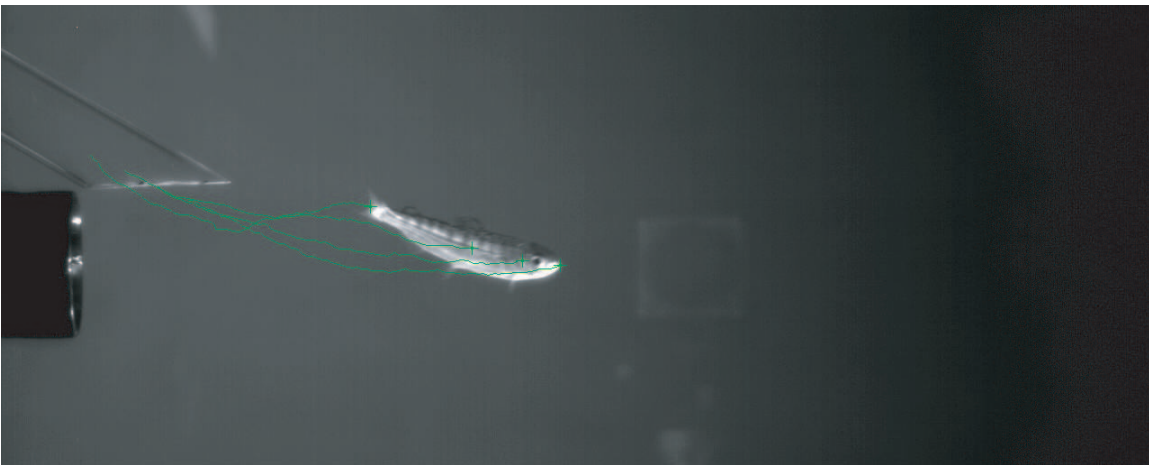
Figure 4.5. A snapshot of motion tracking of fish in a turbulent shear flow.

4.3   Results for bead

Beads were released using the same jet flow apparatus as was used in the PIV experiments. Velocity and acceleration of the beads were computed from trajectory using three methods: unsmoothed, 3-point boxcar simple averaging and 5-point boxcar simple averaging. Theoretically the 5-point boxcar simple averaging method has the smallest error. However, as demonstrated in Figures 4.7 and 4.8, the velocity and acceleration calculation are not sensitive to the smoothing methods, and good agreement between the different smoothing methods can be achieved. Therefore, it is fair to state that the bead-tracking measurements in this test are accurate.

Error analysis was conducted for the 5-point box car averaging method. Only associated random errors are considered as a result of the assumption that the systematic errors are relatively small compared with the random errors. Figures 4.9 and 4.10 include the estimated measurement errors of the velocity and acceleration, and as shown, the relative measurement errors are small for this application with the experimental methods described above.
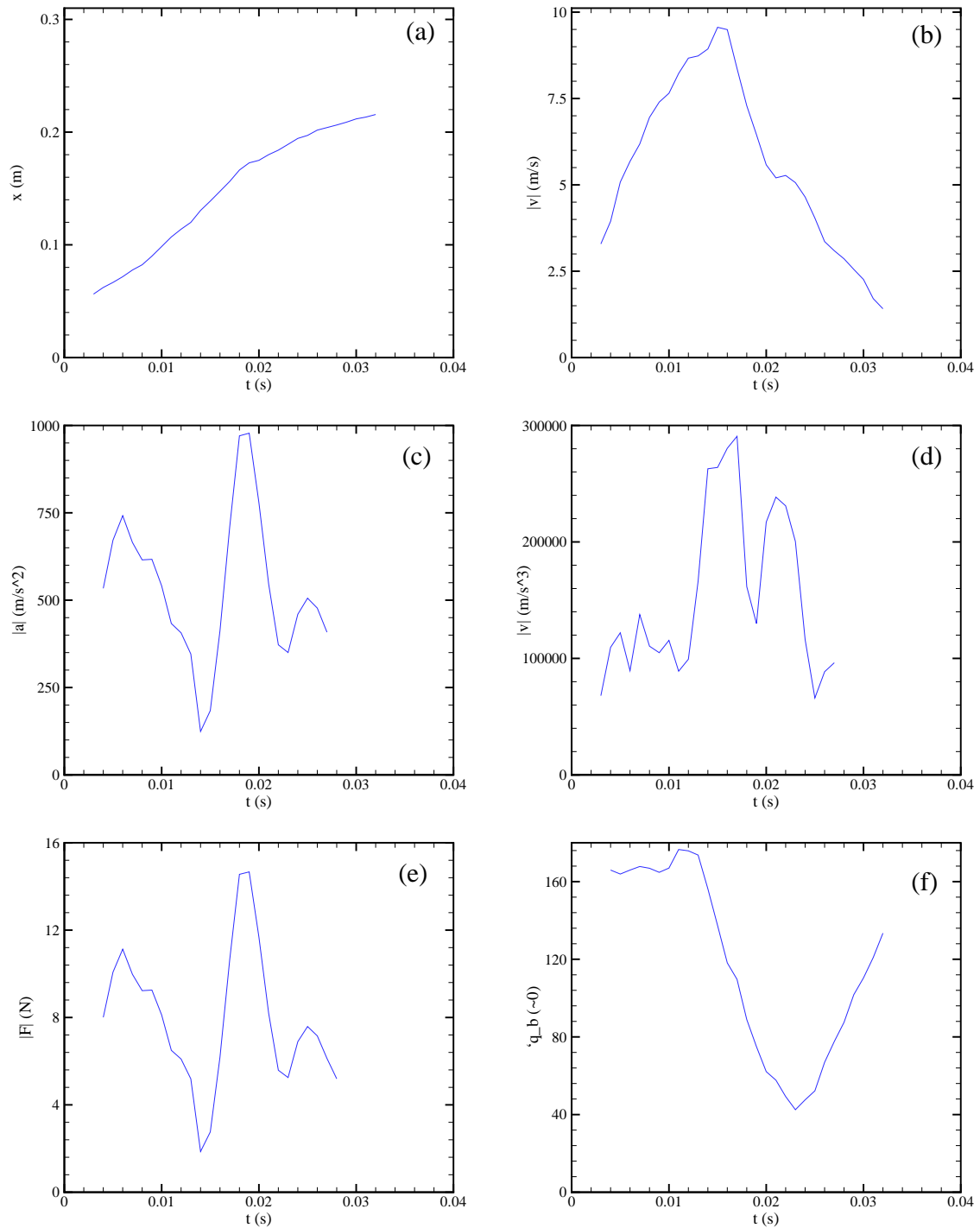
Figure 4.6. Motion analysis results of a release at a nozzle speed of 19.8 m/s: (a) streamwise location; (b) velocity; (c) acceleration; (d) jerk; (e) force; (f) bending.
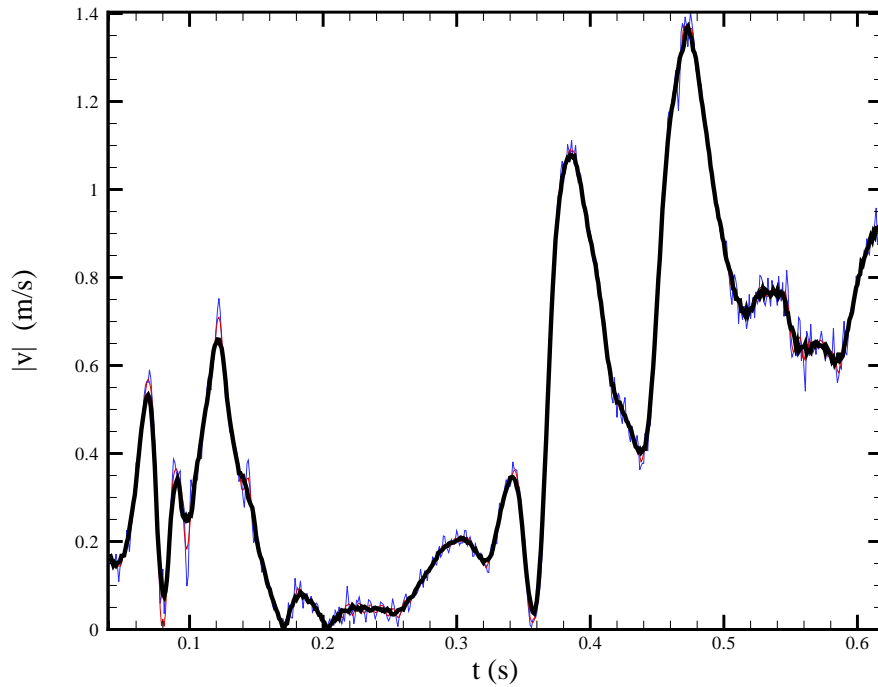
Figure 4.7. Velocity of a bead released around a jet flow in a water tank, with different smoothing methods.
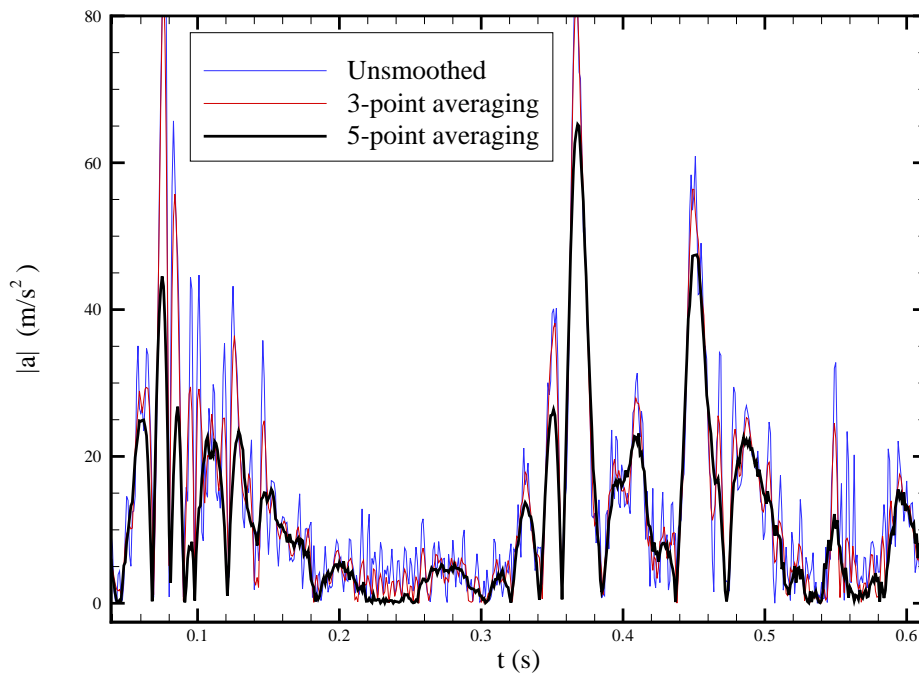
Figure 4.8. Acceleration of a bead released around a jet flow in a water tank, with different smoothing methods.
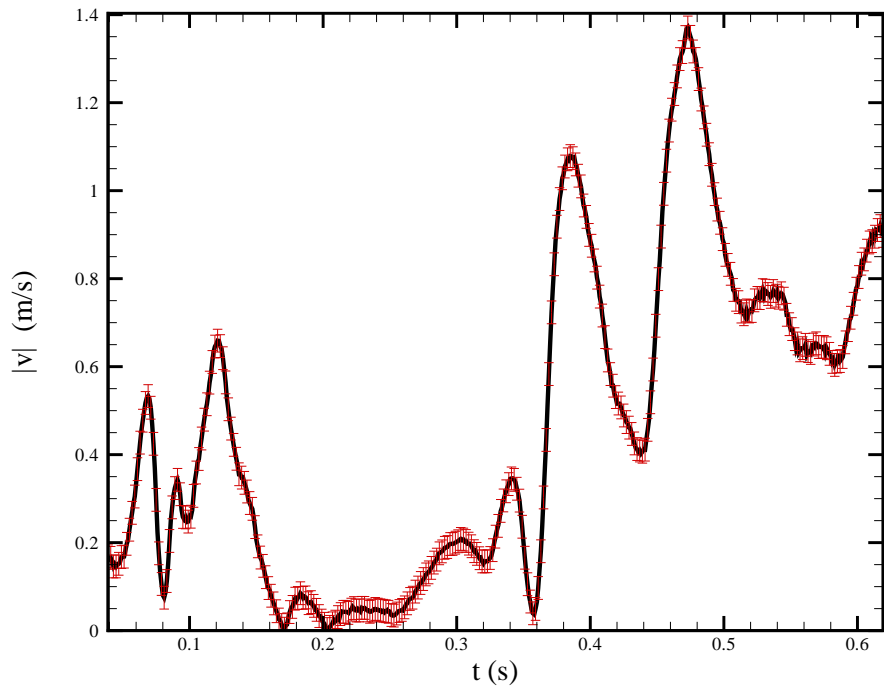
Figure 4.9. Velocity of a bead released around a jet flow, plotted with measurement errors.
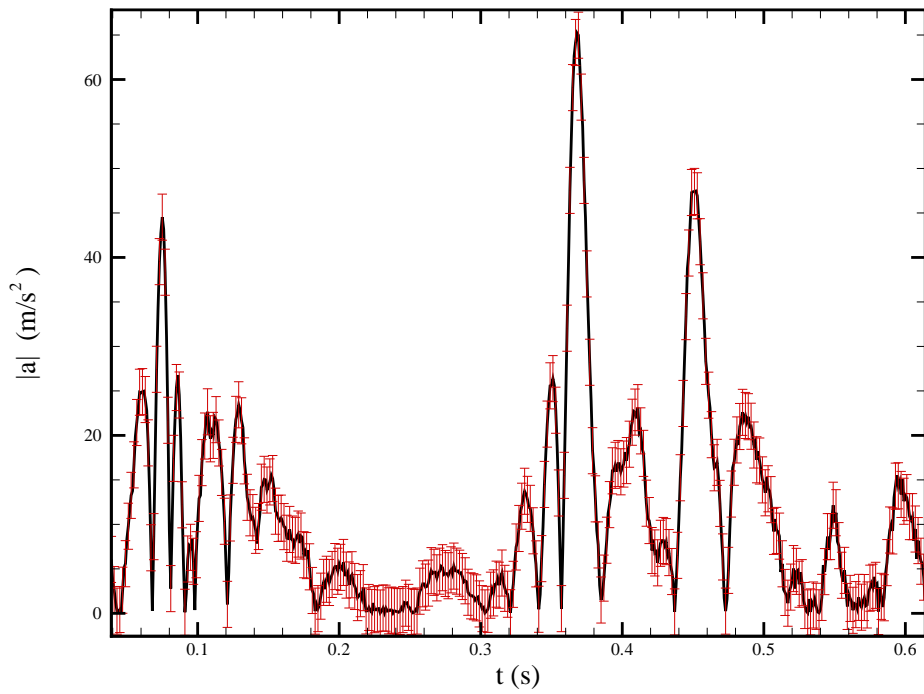
Figure 4.10. Acceleration of a bead released around a jet flow, plotted with measurement errors.

5.0 Recommendations: Research Areas of Interest

The DOE Hydropower Program supports the development of environmentally sound hydro-electric resources, which require understanding of fish injury mechanisms associated with different sources. Currently identified possible sources include cavity, pressure, shear and turbulence, and mechanical injuries. Among these causes, cavity and pressure are the best understood and have lesser physical damage to fish than shear/turbulence and mechanical injuries associated with collisions.

Several laboratory studies (Neitzel et al. 2000; Deng et al. 2004a) have been carried out to investigate the effects of shear on juvenile fish. High-speed imaging and advanced motion analysis techniques were employed to gain information to support a more quantitative analysis of the dynamic parameters involved, such as displacement, orientation, deformation, velocity, acceleration, impulse, force, and jerk etc. The analysis of these parameters emphasized the information relevant to future bio-mechanical testing of fish injury thresholds. However, with PIV, the physical properties related to fish injuries can be defined in an instantaneous fashion, with fine spatial and temporal resolution, for the whole region around the fish body as well as the specific regions of interest. The laboratory results can then be incorporated into a geometry-based computational fluid-structure interaction model that can simulate the complex hydraulic conditions in hydropower systems and their effect on fish, making significant contributions to the development of CFD as a bio-hydraulic design tool.

It is very important ecologically and commercially to understand how fish adapt to or exploit environmental turbulence and change to different thrust-production mechanisms. In addition, in the case of the fish's failure to adapt to the environmental disturbances, the physical properties of the flow field and kinematic response can provide valuable information toward establishing fish injury criteria. However, very little literature exists due to the challenging nature of characterizing kinematic response and the difficulty of defining the environmental perturbations.

Based on existing literature, our technological capability, and relevance and practicability to DOE Hydropower Program, we identified three major research areas of interest: collisions, High shear/turbulence, and Sensor Fish. We propose that the highest priority is to characterize the kinematic response of fish and sensor fish to different turbulent environments such as high shear/turbulence and hydrodynamic disturbances created by solid structures such as deflector and turbine runner blade. The next priority is to correlate the responses of live fish and sensor fish.

The interaction between aquatic animals and water is highly dependent on Reynolds numbers. As discussed earlier, for small Reynolds numbers, viscosity dominates; for very high Reynolds numbers, inertia dominates and three-dimensional complexity occurs. Numerous studies have discussed fish's free swimming, with the majority dealing with the lower end of the Reynolds number range. The Reynolds number for a steady swimming fish of approximately 100 mm body length is usually greater than 10,000 and produces a hydrodynamic trail (wake) consisting of a series of vortex rings. In this range, Both viscosity and inertia need to considered, and three-

37

dimensionality has yet to dominate. The fish of our interest, such as rainbow trout and spring and fall chinook salmon, fall into this category. Detailed information about their swimming behavior can provide the basis for how they react to environmental turbulence or other disturbances.

Because grid turbulence and Kármán vortex street, have been well established and documented in numerous engineering literature and are representative of fish's swimming environments, they will be employed to investigate the effects of environmental disturbances on the swimming behavior of fish. More importantly, extreme conditions which are characteristic of the turbine environment fish could experience in reality, such as high shear/turbulence environments and strike, will be examined. Strike is the collision of fish with solid structures including the runner blade, stay vanes, wicket gates, draft tube piers, baffle blocks, and deflectors on spillways. Very few experimental studies of boundary layer around fish have been conducted due to past technological limitations and complexity of the approach. With high-speed, high-resolution PIV technique, it is possible to characterize the nature of boundary layer around fish, which can lead to significant improvement in the understanding of drag and thrust production mechanisms. Emphasis will be given to the mapping of the boundary layers over juvenile fish swimming behind grid turbulence or in Kármán vortex street.

In field studies, the fish injury mechanisms are complicated by the combinations of various sources of injury, in contrast, through controlled laboratory studies, the contributions to the injury from different sources can be evaluated individually, using the digital PIV system together with our other available techniques such as high-speed photography and advanced motion analysis. By gaining direct knowledge of the biological responses of fish under such extreme hydraulic environments in which fish may lack the capability to overcome the perturbations and be vulnerable to injury, we could provide better-defined validation cases for numerical codes, improve the accuracy of the prediction capability of numerical models in the turbine environment, and integrate results with the response of the Sensor Fish Device to better understand field results.

6.0 Summary and Conclusions

Development of advanced fish-friendly turbine system requires knowledge of fish injury mechanisms. Biological responses of juvenile fish in turbine environment are particularly important because of the relatively high injuries and mortality rate fish experience when they pass through hydroelectric turbines, with shear/turbulence and mechanical injuries being the most significant and least understood sources.

Since its establishment in the last decade, PIV has overcome the limitation of the traditional single-point velocity measurement techniques and become a state-of-the-art, non-intrusive, whole-flow-field technique, providing instantaneous velocity vector measurements in a whole plane. The use of a stereoscopic PIV approach permits instantaneous measurement of all three velocity components, providing a means to characterize real-time three-dimensional flow structures for areas of interest, such as around the body of a fish.

Existing literature on previous PIV studies of fish swimming focused on performance evaluations of freely swimming fish. For flows around different organisms, the related scales and flow regimes vary significantly. The majority of previous investigations dealt with the lower end of the Reynolds number range, in which viscosity is dominant and other effects are negligible. The fish of interest, to turbine passage in the Pacific Northwest, i.e., juvenile steelhead and chinook salmon, fall into the middle range, in which neither viscosity nor inertia is negligible, and three-dimensional complexity has yet to dominate.

Our laboratory tests demonstrated the applicability of PIV to characterize flows around fish. Our measurements showed unsteady vortex shedding in the wake, and very high vorticity and high stress regions around fish head, with the highest in the pectoral area. Results were consistent with the observations by Neitzel et al. (2000) and Deng et al. (2004), specifically that operculum are most vulnerable to damage from the turbulent shear flow, because they are easily pried open. Thus, large vorticity and shear stress can lift and tear off scales, rupture or dislodge eyes, and damage gills. In addition, the unsteady behavior of the vortex shedding in the wake implies that rate of injury to fish by instantaneous flow structures would likely be much higher than those estimated using the average values of the dynamics parameters.

Three major research areas of interest were identified in this study: kinematic response of fish and sensor fish, effects of high shear/turbulence on fish and sensor fish, and correlation of fish and sensor responses. The most important and relevant to the DOE Hydropower Program is characterizing the kinematic response of fish and sensor fish to different extreme hydraulic environments such as high shear/turbulence and hydrodynamic disturbances created by solid structures such as deflector and turbine runner blades.

Precisely controlled laboratory studies with the PIV system, together with other available techniques such as high-speed photography and advanced motion analysis, allows fish injury mechanisms to be isolated. We can gain first-hand knowledge of the biological effects under such

extreme hydraulic environments, and better understand field results by integrating the laboratory studies with the responses of the Sensor Fish Device.

Due to the difficulty of detailing complex fluid-structure interactions, quantification of fish injury mechanisms in turbine environments has often depended more on numerical modelling than direct measurements. Further refinement of the approach outlined in this study will provide well-defined validation cases and boundary conditions for geometry-based computational fluid-structure interaction modeling and allow simulation of the complex hydraulic conditions in advanced hydropower systems and their effects on fish, greatly enhancing the use of CFD as a bio-hydraulic design alternative.

7.0 References

Adrian RJ. 1991. "Particle imaging techniques for experimental fluid mechanics." *Annual Review of Fluid Mechanics* 23:261–304.

Adrian RJ. 1996. *Bibliography of Particle Velocimetry Using Imaging Methods: 1917-1995*. TAM Reports 817, University of Illinois at Urbana-Champaign.

Adrian RJ, Z Deng, and BJ Balasubraniam. 2003. "PIV Studies Of Solid Rocket Motors Flows." In *Proceedings of the Fifth International Symposium on Particle Image Velocimetry*. Busan, Korea.

Ahlborn B, S Chapman, R Stafford, RW Blake, and DG Harper. 1997. "Experimental Simulation of the Thrust Phases of Fast-Start Swimming of Fish." *The Journal of Experimental Biology* 200:2301–2312.

Anderson EJ, WR Mcgillis, and MA Grosenbaugh. 2001. "The Boundary Layer of Swimming Fish." *The journal of Experimental Biology* 204:81–102.

Batchelor GK. 1967. *An Introduction to Fluid Dynamics*. Cambrdige University Press, Cambridge, UK.

Boeing-SVS I. 2003. *Visual Fusion Reference Manual*. Boeing.

Carlson TJ. 2001. "Proceedings of the Turbine Passage Survival Workshop." Portland, Oregon. Prepared for the U.S. Army Corps of Engineers, Pacific Northwest National Laboratory, Richland, Washington.

Carlson TJ and JP Duncan. 2003. *Evolution of the Sensor Fish Device for Measuring Physical Conditions in Severe Hydraulic Environments*. DOE/ID-11079, U.S. Department of Energy Idaho Operations Office, Idaho Falls, Idaho.

Carlson TJ, JP Duncan, and TL Gilbride. 2003. "The Sensor Fish: Measuring Fish Passage in Severe Hydraulic Conditions." *Hydro Review* XXII:62–69.

Čada GF. 1998. "Better Science Supports Fish-Friendly Turbine Designs." *Hydro Review* XVII:52–61.

Čada GF. 2001. "The Development of Advanced Hydroelectirc Turbines to Improve Fish Passage Survival." *Fishery* 26:14–23.

Čada GF, CC Coutant, and RR Whitney. 1997. *Development of Biological Criteria for the Design of Advanced Hydropower Turbines*. DOE/ID-10578, U.S. Department of Energy Idaho Operations Office, Idaho Falls, Idaho.

Chow YC, O Uzol, J Katz, and C Meneveau. 2002. "An Investigation of Axial Turbomachinery Flows Using PIV in an Optically-Unobstructed Facility."

Deng Z, RJ Adrian, and CD Tomkins. 2002. "Sensitivity of Turbulence in Transpired Channel to Injection Velocity Small-Scale Nonuniformity." *AIAA Journal* 40:2241–2247.

Deng Z, GR Guensch, RP Mueller, CA Mckinstry, and MC Richmond. 2004a. "Evaluation of Fish-Injury Mechanisms During Exposure to Turbulent Shear Flow." *sumbitted to Canadian Journal of Fisheries and Aquatic Sciences*.

Deng Z, MC Richmond, CS Simmons, and TJ Carlson. 2004b. *Six-Degree-of-Freedom Sensor Fish Design: Governing Equations and Motion Modeling*. PNNL-14779, Pacific Northwest National Laboratory, Richland, Washington.

Domenici P and RW Blake. 1997. "The Kinematics and Performance of Fish Fast-Start Swimming." *The Journal of Experimental Biology* 200:1165–1178.

Drucker EG and GV Lauder. 1999. "Locomotor Forces on a Swimming Fish: Three-Dimensional Vortex Wake Dynamics Quantified Using Digital Particle Image Velocimetry." *The Journal of Experimental Biology* 202:2393–2412.

Drucker EG and GV Lauder. 2000. "A Hydrodynamic Analysis of Fish Swimming Speed: Wake Structure and Locomotory Force in Slow and Fast Labriform Swimmers." *The Journal of Experimental Biology* 203:2379–2393.

Drucker EG and GV Lauder. 2001a. "Locomotor Function of the Dorsal Fin in Teleost Fishes: Experimental Analysis of Wake Forces in Sunfish." *The Journal of Experimental Biology* 2004:2943–2958.

Drucker EG and GV Lauder. 2001b. "Wake Dynamics and Fluid Forces of Turning Maneuvers in Sunfish." *The Journal of Experimental Biology* 204:431–442.

Fischer HB, EJ List, RCY Koh, J Imberger, and NH Brooks. 1979. *Mixing in Inland and Coastal Waters*. Academic Press.

Guensch GR, RP Mueller, CA Mckinstry, and DD Dauble. 2002. *Evaluation of Fish-Injury Mechanicsms During Exposure of a High-Velocity Jet*. DOE/ID-11073, U.S. Department of Energy Idaho Operations Office, Idaho Falls, Idaho.

Hanke W, C Brucker, and H Bleckmann. 2000. "The Aging of the Low-Frequency Water Distrubances Caused by Swimming Goldfish and its Possible Relevance to Prey Detection." *The Journal of Experimental Biology* 203:1193–1200.

Hrubes J. 2001. "High-Speed Imaging of Supercavitating Underwater Projectiles." *Experiments in Fluids* 30:57–64.

Hughes N and L Kelly. 1996. "New Techniques for Video Tracking of Fish Swimming Movements in Still or Flowing Water." *Canadian Journal of Fisheries and Aquatic Sciences* 53:2473–2483.

Jones SC and F Sotiropoulos. 2002. *Large-Eddy Simulation of Turbulent Circular Jet Flows*. DOE/ID-10971, U.S. Department of Energy Idaho Operations Office, Idaho Falls, Idaho.

Kang J, V Agaram, G Nusholtz, and G Kostyniuk. 2001. *Air Bag Loading on In- Position Hybrid III Dummy Neck*. Paper 2001- 01-0179, Society of Automotive Engineers, Inc.

Keane RD and RJ Adrian. 1992. "Theory of cross-correlation analysis of PIV images." *Applied Scientific Research* 49:191–215.

Lauder GV. 2000. "Function of the Caudal Fin During Locomotion in Fishes: Kinematics, Flow Visualization, and Evolutionary Patterns." *American Zoologist* 40:101– 122.

Liao J and GV Lauder. 2000. "Function of the Heterocercal Tail in White Sturgeon: Flow Visulaization During Steady Swimming and Vertical Maneuvering." *The Journal of Experimental Biology* 203:3585–3594.

Liao JC, DN Beal, GV Lauder, and MS Traintafyllou. 2003a. "Fish Exploiting Vortices Decrease Muscle Activity." *Science* 302:1566–1569.

Liao JC, DN Beal, GV Lauder, and MS Traintafyllou. 2003b. "The Karman Gait: Novel Body Kinematics of Rainbow Trout Swimming in a Vortex Street." *The Journal of Experimental Biology* 206:1059–1073.

Lighthill MJ. 1973. "On the Weis-Fogh Mechanism of Lift Generation." *Journal of Fluid Mechanics* 60:1–17.

Liu H, CP Ellington, K Kawachi, C Van Den Berg, and A Willmott. 1998. "A Computational Fluid Dynamic Study of Hawkmoth Hovering." *The Journal of Experimental Biology* 201:461– 477.

Liu H, RJ Wassersug, and K Kawachi. 1997. "The Threedimensional Hydrodynamics of Tadpole Locomotion." *The Journal of Experimental Biology* 200:2807–2819.

Liu ZC, RJ Adrian, and TJ Hanratty. 1991. "High resolution measurement of turbulent structure in a channel with particle image velocimetry." *Experiments in Fluids* 10(6):301–312.

Meinhart CD, ST Wereley, and JG Santiago. 1999. "PIV Measurements of a Microchannel Flow." *Experiments in Fluids* 27:414–419.

Muller UK, J Smit, EJ Stamhuis, and JJ Videler. 2001. "How the Body Contributes to the Wake in Undulatory Fish Simming: Flow Fields of a Swimming Eel (Anguilla Anguilla)." *The Journal of Experimental Biology* 204:2751–2762.

Muller UK, EJ Stamhuis, and JJ Videler. 2000. "Hydrodynamics of Unsteady Fish Swimming and the Effects of Body Size: Comparing the Flow Fields of Fish Larvae and Adults." *The Journal of Experimental Biology* 203:193–206.

Müller UK, BLE Van Den Heuvel, EJ Stamhuis, and JJ Videler. 1997. "Fish Foot Prints: Morphology and Energetics of the Wake Behind a Continuously Swimming Mullet (Chelon Labrosus Risso)." *The Journal of Experimental Biology* 200:2893–2906.

Nauen JC and GV Lauder. 2002a. "Hydrodynamics of Caudal Fin Locomotion by Chub Mackerel, Scomber Japonicus." *The Journal of Experimental Biology* 205:1709– 1724.

Nauen JC and GV Lauder. 2002b. "Quantification of the Wake of Rainbow Trout (Oncorhynchus Mykiss) Using Three-Dimensional Stereoscopic Digital Particle Image Velocimetry." *The Journal of Experimental Biology* 205:3271–3279.

Neitzel DA, DD Dauble, GF Ćada, MC Richmond, GR Guensch, RP Mueller, CS Abernethy, and B Amidan. 2004. "Survival Estimates for Juvenile Fish Subjected to a Laboratory-Generated Shear Environment." *Transactions of the American Fisheries Society* 133:447–454.

Neitzel DA, MC Richmond, DD Dauble, RP Mueller, RA Moursund, CS Abernethy, GR Guensch, and GF Ćada. 2000. *Laboratory Studies on the Effects of Shear on Fish: Final Report.* DOE/ID-10822, U.S. Department of Energy Idaho Operations Office, Idaho Falls, Idaho.

Prasad AK, RJ Adrian, CC Landreth, and PW Offutt. 1992. "Effect of resolution on the speed and accuracy of particle image velocimetry interrogation." *Experiments in Fluids* 13(2):105–116.

Raffel M, C Willert, and J Kompenhans. 1998. *Particle Image Velocimetry: A Practical Guide.* Springer, New York.

Ramamurti R, WC Sandberg, R Lohner, JA Walker, and MW Westneat. 2002. "Fluid Dynamics of Flapping Aquatic Flight in the Bird Wrasse: Three-Dimensional Unsteady Computations with Fin Deformation." *The Journal of Experimental Biology* 205:2997–3008.

Stamhuis EJ and JJ Videler. 1995. "Quantitative Flow Analysis Around Aquatic Animals Using Laser Sheet Particle Image Velocimetry." *The Journal of Exeperimental Biology* 198:283–294.

Stamhuis EJ and JJ Videler. 1998. "Burrow Ventilation in the Tube Dwelling Shrimp Callianassa Subteranea (Decapoda, Thalassinidea)." *The Journal of Experimental Biology* 201:2159–2170.

Stamhuis EJ, JJ Videler, LA Van Duren, and UK Muller. 2002. "Applying Digital Particle Image Velocitymetry to Animal-Generated Flows: Traps, Hurdles and Cures in Mapping Steady and Unsteady Flows in Re Regimes Between 10^{-2} and 10^5." *Experiments in fluids* 33:801–813.

Tanaka K, M Nishida, T Kunimochi, and T Takagi. 2002. "Discrete Element Simulation and Experiment for Dynamic Response of Two-Dimensional Granular Matter to the Impact of a Spherical Projectile." *Powder Technology* 124:160–173.

Tang M, D Bosclair, C Ménard, and J Downing. 2000. "Influence of Body Weight, Swimming Characteristics, and Water Temperature on the Cost of Swimming in Brook Trout (Salvelinus Fontinalis)." *Canadian Journal of Fisheries and Aquatic Sciences* 57:1482–1488.

Ten Cate A, CH Nieuwstad, JJ Derksen, and HAE Van Den Akker. 2002. "Particle Imaging Velocimetry Experiements and Lattice-Boltzmann Simulations on a Single Sphere Settling under Gravity." *Physics of Fluids* 14(11):4012–4025.

Uijttewaal WSJ, V Weitbrecht, CF Graf Von Cramer, and JH Jirka, eds.. 2001. *Experiments on Shallow Flow Turbulence.* ISEH and IAHR.

Van Duren LA, EJ Stamhuis, and JJ Videler. 2003. "Copepod Feeding Currents: Flow Patterns, Filtration Rates and Energetics." *Journal of Experimental Biology* 206:255–267.

Van Duren LA and JJ Videler. 2003. "Escape from Viscocity: The Kinematics and Hydrodynamics of Copepod Foraging and Escape Swimming." *The Journal of Experimental Biology* 206:269–279.

Videler JJ. 1993. *Fish Swimming.* Chapman & Hall, London.

Videler JJ, EJ Stamhuis, UK Muller, and LA Van Duren. 2002. "The Scaling and Structure of Aquatic Animal Wakes." *Ingegr. Comp. Biol.* 42:988–996.

Webb PW. 1988. "Simple Physical Principles and Vertebrate Aquatic Locomotion." *American Zoologist* 28:709–725.

Zhu Q, MJ Wolfgang, DKP Yue, and MS Triantafyllou. 2002. "Three-Dimensional Flow Structures and Vorticity Control in Fish-Like Swimming." *J. Fluid Mech.* 468:1–28.

Appendix A

Animations of PNNL PIV and High-Speed, High-Resolution Imaging Measurements

Appendix A – Animations of PNNL PIV and High-Speed, High-Resolution Imaging Measurements

Animations of instantaneous velocity, vorticity, and exposure strain rate experienced by fish in turbulent shear flow, and advanced motion analysis of fish and Sensor Fish are included as .avi files on the compact disc included with the report.